nature communications

Article

https://doi.org/10.1038/s41467-026-70479-z

IL-17RA signaling promotes the dedifferentiation of Paneth progenitors through ADAM17 to regenerate gut epithelium post-irradiation

Received: 18 June 2025

Accepted: 23 February 2026

Published online: 17 March 2026

Check for updates

Cody G. Kempen[1], Ankita Singh[1], Keith A. Breau[2], Hafiz I. Tariq[1], Yangle Yu[1], Stephen J. Gaudino[1], Tej Bahadur[1], Emilia Orzechowska-Licari[3], Onur Eskiocak[4], Kiyoshi Shiomitsu[1], Richard Blumberg[5], Paula Denoya[6], Rebecca Martin[7], Agnieszka B. Bialkowska[8], Semir Beyaz[4], Scott T. Magness[2,9,10,11], Patrick Hearing[1], Hwan Keun Kim[1], Brian S. Sheridan[1], Peter Dempsey[12] & Pawan Kumar[1]

Paneth cells and their antimicrobial products are critical in mediating small intestinal host defense under homeostatic conditions and after injury or infection. In addition, Paneth cells have also been shown to gain stem-like properties and repropagate intestinal crypts after intestinal injury. The specific role of intestinal IL-17A or its receptor (IL-17RA) signaling in Paneth cells to gain stem-like features has yet to be investigated. Using Paneth cell-specific IL-17RA (*Il17ra*$^{fl/fl}$*;Defa6-cre*) knockout mice, anti-IL-17A neutralizing studies and lineage tracer (*Defa6-cre;mT/mG)* mice, we show that after injury IL-17RA signaling is required for Paneth cell to gain stem-like properties to regenerate the intestinal epithelium. Increased susceptibility of *Il17ra*$^{fl/fl}$*;Defa6-cre* mice is associated with reduced expression *Adam17* in the terminal ileum. *Adam17* overexpression in *Il17ra*$^{fl/fl}$;*Defa6-cre* mice rescues the epithelial regeneration defect in these mice. IL-17A induces Nox1 in Paneth cells and H_2O_2 induces ADAM17 enzymatic activity. Finally, using Paneth cell-specific *Adam17* (*Adam17*$^{fl/fl}$*;Defa6-cre*) knockout mice, we show that ADAM17 in Paneth cells is required for tissue regeneration. Collectively, our data reveal an essential role of the IL-17RA-ADAM17 pathways in Paneth cells for tissue regeneration.

Paneth cells are highly specialized cells vital for regulating microbiota homeostasis, instituting protective antimicrobial processes, and providing a niche for developing stem cells[1–4]. They are localized at the base of intestinal crypts. Patients with Crohn's Disease (CD), a form of inflammatory bowel disease (IBD), exhibit abnormalities and impaired antimicrobial processes within their Paneth cells[5]. A hallmark of Paneth cells is their large, dense secretory granules. These granules store various antimicrobial peptides used to regulate the host microbiota and defend against invading pathogens[6–8]. Paneth cells also play a vital role in maintaining the intestinal stem cell (ISC) niche. They produce epidermal growth factor (EGF) and selective WNTs, which help support the self-renewal and survival of Lgr5^{+} ISCs[2,7]. After intestinal injury, it has been reported that other intestinal epithelial cell types, including Paneth cells, can dedifferentiate and replenish the intestinal crypt[9–12]. This process is dependent on the activation of multiple pathways. Notch signaling through notch intracellular domain (NICD) activation

A full list of affiliations appears at the end of the paper. e-mail: pawan.kumar@stonybrook.edu

has been implicated in Paneth cell dedifferentiation and proliferation[10,12]. Simultaneously, it was reported that stem cell factor (SCF) signaling to c-Kit in response to inflammation causes Paneth cell dedifferentiation through activation of the PI3K/AKT signaling axis[9]. While IL-17RA is expressed on the intestinal epithelium, including Paneth cells[13,14], it is not known if immune cell-derived factors such as IL-17A regulate Paneth cell dedifferentiation.

The IL-17 family of cytokines is widely studied and plays an important role in immunity and inflammation[15]. While the family consists of 6 signaling molecules (IL-17A-F), IL-17A and IL-25 (formerly known as IL-17E) are the best characterized[15,16]. IL-17A signals primarily through the IL-17RA/RC co-receptor complex. IL-17RA is expressed widely across mammalian tissue, while IL-17RC expression is restricted to epithelial, mesenchymal cells and a few other cell types[17]. Since IL-17A can signal to many cell types throughout the body, its expression and production are tightly controlled. Increased expression of IL-17A can be a contributing factor to autoimmune diseases, such as plaque psoriasis[18,19]. Increased amounts of IL-17A are also found in the intestinal mucosa of patients suffering from IBD[20]. Anti-IL-17A or anti-IL-17RA therapies commonly used to treat plaque psoriasis patients were unsuccessful in treating IBD and, in some instances, worsened the disease[20,21]. We and others have shown that IL-17A is vital in maintaining intestinal barrier integrity after injury and promoting gut microbiota homeostasis[22–25]. Recently, we have shown that IL-17A signaling within the gut, specifically to Lgr5$^+$ stem cells, promotes secretory lineage commitment at a steady state[13]. While a beneficial role for IL-17A signaling within the gut has been established, the role of IL-17A signaling to specific intestinal epithelial cell types is still an area of active research. After injury, several epithelial cell types, including Paneth cells, endocrine, and enterocytes, gain stem-like properties to regenerate the gut epithelium[9,26,27]. Almost nothing is known at present whether IL-17A promotes or inhibits epithelial cell stem-like properties.

Our findings suggest that while, loss of IL-17RA signaling to Paneth cells is insignificant under homeostasis, however, the ability of Paneth cells to dedifferentiate and replenish the intestinal crypt after injury depends on IL-17RA. Utilizing our whole-body IL-17RA knockout (*Il17ra*^{KO}) and *Il17ra*$^{fl/fl}$*;Villin-cre* mice, we show a lack of IL-17RA signaling to the intestinal epithelium leads to systemic bacterial dissemination to the spleen and liver after lethal doses of irradiation. This is compounded by significant structural damage and inflammation within the gut of these mice. This phenotype is recapitulated within our *Il17ra*$^{fl/fl}$*;Defa6-cre* mice, showing the importance of IL-17RA signaling to Paneth cells in recovering from injury. Neutralizing IL-17A in irradiated Paneth cell lineage tracer (*Defa6-cre;mT/mG*) mice reduces stemness and epithelial regeneration. We show that continuous stimulation of organoids grown from Paneth cell lineage tracer mice with IL-17A increases the number of Paneth cells in organoid buds after irradiation. Furthermore, a subset of these Paneth cells gains stemlike properties and can develop into new organoids after passage. We found reduced expression of *Adam17* in the terminal ileum of irradiated *Il17ra*$^{fl/fl}$*;Defa6-cre*+ mice. Furthermore, sorted Paneth cells from irradiated Paneth cell lineage tracer organoids treated with IL-17A showed increased expression of *Adam17* and *Nox1*. NOX1 regulates epithelial redox, and H_2O_2 enhances ADAM17 enzymatic activity. Using *Adam17*$^{fl/fl}$*;Defa6-cre*+ mice, mechanistically, we show that epithelium, including Paneth cell-based, intestinal regeneration is linked to the IL-17A-ADAM17 axis.

Results

Loss of intestinal IL-17RA signaling promotes intestinal bacterial dissemination to the spleen and liver

Radiation injury is a well-established model to study Lgr5$^+$ stem cell-independent epithelial regeneration as it ablates actively proliferating stem cells[26]. C57BL/6 (WT) and whole-body IL-17RA knockout (*Il17ra*^{KO}) mice were irradiated at 12 Gy and returned to their cages. This dose of irradiation promotes intestinal epithelial cell damage and widespread death of Lgr5$^+$ ISCs and transit-amplifying (TA) cells within crypts[28]. Mice were sacrificed 5 days post-irradiation, and tissues were collected. Hematoxylin and eosin (H&E) staining of terminal ileal tissue from irradiated *Il17ra*^{KO} mice revealed greater structural damage and inflammation compared to WT mice. Specifically, we measured the length of the crypt/villi structure. We measured from the base of the crypt to the top of the villi and observed shortening of the crypt/villi structure in irradiated *Il17ra*^{KO} mice as compared to *WT* mice (Fig. 1A). Their liver and spleen were harvested, homogenized, and plated. After 48 hours, colonies were counted. We observed significant growth of bacterial colonies from spleen and liver tissues taken from *Il17ra*^{KO} mice when compared to tissues from WT mice (Fig. 1B). Along with this, there was increased Lipocalin-2 (LCN2) in the cecal contents of *Il17ra*^{KO} mice compared to WT mice (Fig. 1C). LCN2 is a siderophore known to help control microbiota dysbiosis and used as a marker for intestinal inflammation[29]. While LCN2 can be induced by IL-17A, it can also be induced by a plethora of inflammatory stimuli (e.g., LPS) and cytokines (e.g., IL-6, IL-10, and IL-22)[30]. To determine whether the loss of IL-17RA signaling affected proliferation within the intestinal villi, we performed immunofluorescence (IF) staining and stained tissue for proliferating cell nuclear antigen (PCNA). Results showed reduced proliferation in the ileum of *Il17ra*^{KO} mice compared to *WT* mice (Fig. 1D). To rule out hematopoietic failure contribution to an observed phenotype, bone marrow from non-irradiated WT and *Il17ra*^{KO} mice were transplanted into their irradiated counterparts 2 hours post-irradiation (Fig. 1E). We observed a significant increase in systemic bacterial dissemination in *Il17ra*^{KO} mice compared to their WT counterparts (Fig. 1F). To further explore IL-17RA signaling within the intestines, we used intestinal epithelial-specific IL-17RA knock-out mice (*Il17ra*$^{fl/fl}$*;Villin-cre* +/−). Irradiated *Il17ra*$^{fl/fl}$*;Villin-cre* + mice similarly showed greater structural damage and increased bacterial dissemination to the spleen and liver than their *cre-* counterparts (Fig. 1G, H). We also observed a trend towards increased LCN2 in the cecal content of irradiated *Il17ra*$^{fl/fl}$*;Villin-cre* + mice (Fig. 1I). Lastly, we also observed reduced cellular proliferation in the ileum of *cre*+ mice as compared to *cre-* mice (Fig. 1J). Taken together, these observations show that a lack of intestinal IL-17RA signaling resulted in gut barrier or epithelial regenerative defects.

Rapid depletion of Lgr5$^+$ stem cells does not compromise intestinal regeneration following irradiation-induced injury

A prior study showed that Lgr5$^+$ cells are indispensable for tissue recovery after radiation-induced injury[31]. It is also well established in the literature that radiation readily kills Lgr5$^+$ stem cells[28,32,33]. Utilizing *Lgr5-EGFP-cre*^{ERT2}*;RosaLSLTdtomato* mice, we confirmed that radiation ablated Lgr5$^+$ cells in the small intestine, which then reappear 7 days post irradiation (Fig. 2A, B). Once the involvement of Lgr5$^+$ stem cells was ruled out, we then investigated which other cell type may mediate IL-17RA-induced protection. To do this, we screened for changes in RT-qPCR data from post-irradiated *Il17ra*^{KO} mice. Results revealed decreased expression of the Paneth cell marker *Lyz1*. We saw no differences in the expression of markers for other intestinal epithelial cells, such as *Muc2* (goblet cells), clusterin (*Clu*), a marker for a type of quiescent intestinal stem cells, and fetal-like markers including *Anxa1, Anxa3, Anxa5, Ly6A*, and *Ly6D*. (Fig. 2C). To confirm this expression data, we stained *Il17ra*^{KO} and *Il17ra*$^{fl/fl}$*;Villin-cre* + mice for Lyz1. We saw reduced amounts of Lyz1 in the ileum of both subsets of mice as compared to their *WT* and *cre-* counterparts (Fig. 2D, E). Since we observed decreased expression of *Lyz1* in irradiated *Il17ra*^{KO} mice, followed by decreased amounts of Lyz1 in both *Il17ra*^{KO} and *Il17ra*$^{fl/fl}$*;Villin-cre* + mice, we decided to study the role of IL-17RA signaling in Paneth cells.

https://doi.org/10.1038/s41467-026-70479-z

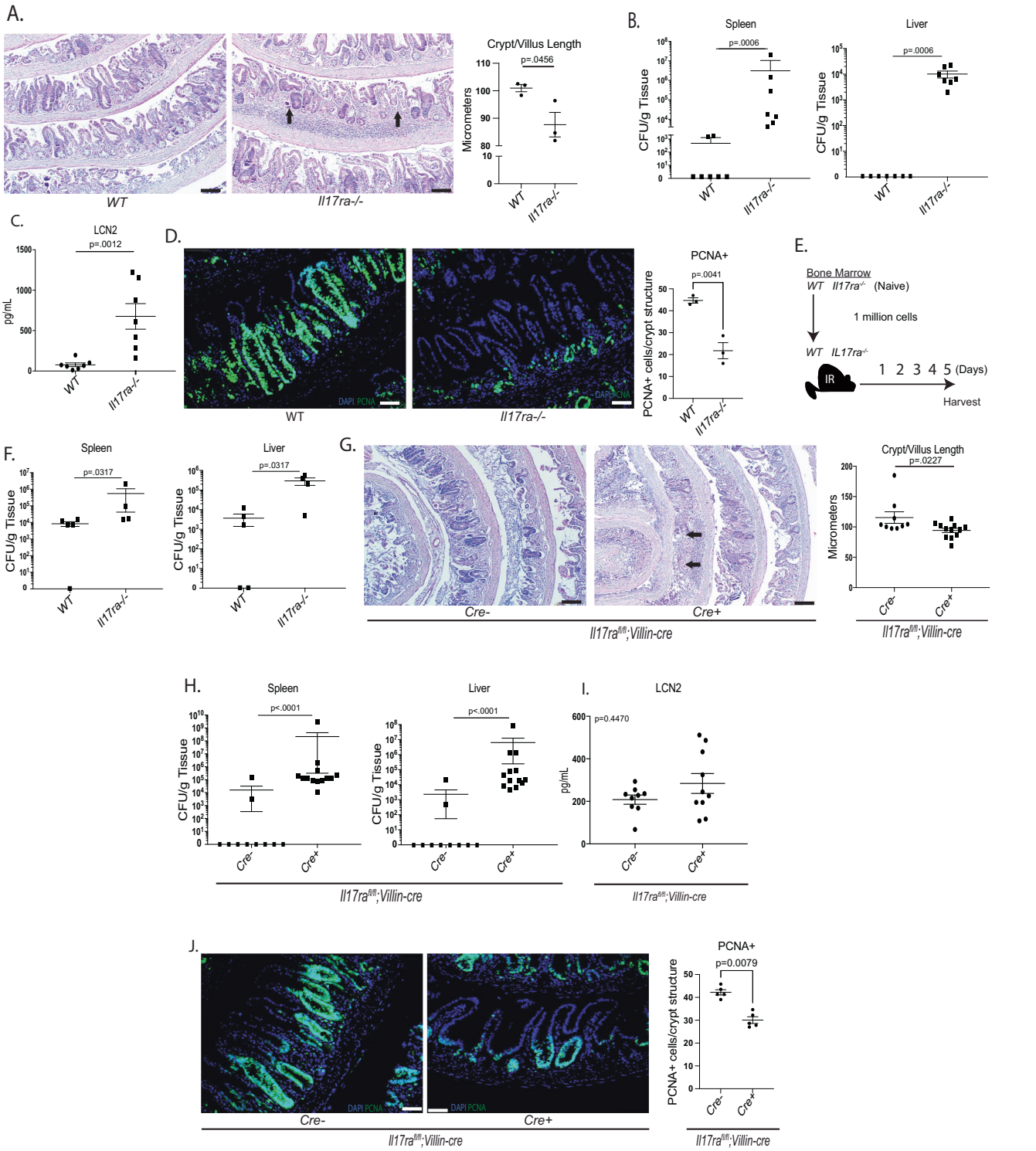

During homeostasis loss of IL-17RA signaling to Paneth cells does not alter their function

To study the importance of IL-17RA signaling in Paneth cells, we generated *Il17ra*$^{fl/fl}$*;Defa6-cre* mice, which lack IL-17RA specifically on Paneth cells (Supplementary Fig. S1A)[13]. We extensively characterized naïve *Il17ra*$^{fl/fl}$*;Defa6-cre* mice. RNA-seq data from ileum tissues *Il17ra*$^{fl/fl}$*;Defa6-cre* + /- mice showed no significant alterations in the expression of antimicrobial peptides or stem cell genes (Supplementary Fig. S1B). To validate this data, we performed RT-qPCR of Paneth cell-related genes from ileum tissue of *Il17ra*$^{fl/fl}$*;Defa6-cre* + /− mice, which did not show significant differences in expression between *cre-*/+ mice (Supplementary Fig. S1C). Furthermore, IF staining for Lyz1 in *Il17ra*$^{fl/fl}$*;Defa6-cre* + /− mice showed no differences in the number of Lyz1^{+} Paneth cells (Supplementary Fig. S1D). We show that Paneth cells of *Il17ra*$^{fl/fl}$*;Defa6-cre* + /− mice display similar morphology and secretory vesicle number via transmission electron microscopy of ileal tissues (Supplementary Fig. S1E). Acid Urea (AU) PAGE electrophoresis was performed to determine changes in cryptidin levels between *Il17ra*$^{fl/fl}$*;Defa6-cre* + /− mice. AU-PAGE is a unique form of protein electrophoresis that separates proteins based on their charge. Results indicated no differences in cryptidin protein levels between *cre-* and *cre* + mice (Supplementary Fig. S1F). Lastly, 16S microbial sequencing

Fig. 1 | Loss of intestinal integrity after irradiation in the absence of IL-17RA signaling. A Representative images of hematoxylin and eosin staining of the terminal ilea from wild type and *Il17ra*^{KO} mice 5 days after irradiation (scale bar = 100 µm) (left). Arrows represent areas of damage. Quantification of crypt lengths (right). Mice were 13 and 14 weeks old. *N* = 6. **B** Splenic and hepatic bacterial dissemination in wild-type and *Il17ra*^{KO} mice 5 days after irradiation. Mice were 13 and 14 weeks old. *N* = 14. **C** Amounts of lipocalin in the cecal content of irradiated wild-type and *Il17ra*^{KO} mice measured via ELISA. Mice were 13 and 14 weeks old. *N* = 14. **D** Representative immunofluorescent images depicting PCNA (green) and DAPI (blue) from the terminal ilea of wild type and *Il17ra*^{KO} mice 5 days after irradiation (scale bar = 50 µm) (left) and quantification (right). Mice were 13 and 14 weeks old. *N* = 6. **E** Schematic of bone marrow transplantation and irradiation procedure. **F** Splenic and hepatic bacterial dissemination in bone marrow transferred wild-type and *Il17ra*^{KO} mice 5 days after irradiation. Mice were 8 and 11 weeks old. *N* = 9. **G** Representative images of hematoxylin and eosin staining of terminal ilea from *Il17ra*$^{fl/fl}$*;Villin-cre* + /− mice 5 days after irradiation (scale bar = 100 µm) (left). Arrows represent areas of damage. Quantification of crypt lengths (right). Mice were 7.2, 7.4, 10 and 14.6 weeks old. *N* = 21. **H** Splenic and hepatic bacterial dissemination in *Il17ra*$^{fl/fl}$*;Villin-cre* + /− mice 5 days after irradiation. Mice were 7.2, 7.9, and 14.6 weeks old. *N* = 23. **I** Amounts of lipocalin in the cecal content of irradiated *Il17ra*$^{fl/fl}$*;Villin-cre* + /− mice measured via ELISA. Mice were 7.2, 7.9, and 14.6 weeks old. *N* = 19. **J** Representative immunofluorescent images depicting PCNA (green) and DAPI (blue) from the terminal ilea of *Il17ra*$^{fl/fl}$*;Villin-cre* + /− mice 5 days after irradiation (scale bar = 50 µm) (left) and quantification (right). Mice were 7.9, and 14.6 weeks old. *N* = 10. *N* = number of biologically independent mice. All figures are generated from 3 experiments. Data in Fig. 1A, D was analyzed via Students *t* test. Data are presented as ± SEM on relevant graphs. (Mann-Whitney test, Two-tailed and Student's *T* test).

revealed no changes in microbiota between naïve *cre*- and *cre* + mice (Supplementary Fig. S1G). Collectively, our data indicate that loss of IL-17RA signaling to Paneth cells does not alter their function under homeostatic conditions.

IL-17RA signaling, specifically to Paneth cells, promotes intestinal integrity after irradiation-induced injury

We then characterized *Il17ra*$^{fl/fl}$*;Defa6-cre* mice after irradiation-induced injury. Our results were similar to those observed in *Il17ra*^{KO} and *Il17ra*$^{fl/fl}$*;Villin-cre* mice. There was shortening of crypt/villi length within the ileum of *cre*+ mice 3 days post irradiation (Fig. 3A). Five days post irradiation injury, there was increased bacterial dissemination to the spleen and liver in *Il17ra*$^{fl/fl}$*;Defa6-cre* + mice as compared to *cre*- mice (Fig. 3B). This was coupled with increased LCN2 concentrations within *cre* + cecal contents (Fig. 3C). Utilizing an anaerobic chamber, we also observed increased anaerobic bacterial dissemination to the spleen and liver in *Il17ra*$^{fl/fl}$*;Defa6-cre* + mice (Supplementary Fig. S1H). The presence of cecal albumin was indicative of gut barrier injury (Supplementary Fig. S1I). Immunofluorescence staining of PCNA revealed decreased cellular proliferation in *Il17ra*$^{fl/fl}$*;Defa6-cre* + mice compared to *cre*- mice post-irradiation injury (Fig. 3D). We next wanted to determine if the regeneration canonical ISCs was impaired in *Il17ra*$^{fl/fl}$*;Defa6-cre* + mice after irradiation. As expected, we saw reduced amounts of Olfm4 + crypts in mice 5 days post- irradiation as compared to non-irradiated mice. Interestingly, we also observed decreased amounts of Olfm4 + crypts in irradiated *Il17ra*$^{fl/fl}$*;Defa6-cre* + mice as compared to irradiated *cre*- mice. This revealed that canonical ISCs regeneration was indeed impaired in *Il17ra*$^{fl/fl}$*;Defa6-cre* + mice as compared to *cre*- mice 5 days post irradiation (Fig. 3E). We did not observe a difference in the number of Lyz1^{+} Paneth cells between *cre*- and *cre*+ mice post irradiation (Supplementary Fig. S1J). Immune profiling revealed a lack of differences between populations of adaptive immune cells in the lamina propria of irradiated *cre*- and *cre* + mice (Supplementary Fig.S2A). However, total cell numbers of ILC1s were significantly greater in the lamina propria of irradiated *cre*+ mice as compared to *cre*- mice (Supplementary Fig. S2B). We also show that there are equivalent amounts of IL-17A producing ILC3s and CD3+ cells within the lamina propria of irradiated *cre*- and *cre* + mice (Supplementary Fig. S2C, D). Furthermore, there was no difference in key IL-17A inducible chemokine (*Cxcl5, Ccl2* and *Cxcl1*) expression within the ilea of irradiated *cre*- and *cre* + mice (Supplementary Fig. S2E). Commensal microbiota have been shown to promote intestinal regeneration[34]. Subsets of commensal microbiota expand at sites of intestinal injury and promote wound healing[35]. We first compared the *Il17ra*$^{fl/fl}$*;Defa6-cre* + /- mice microbiota in the non-irradiated control group. When observing beta diversity at the phylum, family, genus, and species level, there was no distinct clustering between groups. This indicates that with the Weighted UniFrac metric, these groups are more similar than dissimilar at each phylogenetic level. Further, when performing LEfSe, no phylum, family, genus, or species were identified as significantly different in abundance between the cre + /- non-irradiated mice, even with an LDA cut-off of 1, and a p-value of 0.10 (Fig. 3F–I). While the microbiota composition changed after irradiation, the difference was subtle for both *cre*- and *cre* + mice (Fig. 3J–M). These results suggest that IL-17RA signaling to Paneth cells is vital in limiting damage in response to irradiation, independent of microbiota regulation.

Subsets of Paneth progenitors express high levels of IL-17RA and IL-17RC

We have previously shown via single-cell RNA-sequencing (scRNA-seq) of enteroids that a small subset of Paneth cells expresses IL-17RA, while secretory progenitors express the highest levels of IL-17RA[13]. To investigate this deeper, we analyzed a previously published single-cell RNA sequencing data set enriched for primary murine Paneth cells (PMID: 29144463), which identified three distinct subsets of Paneth cells (Paneth 1, Paneth 2, Paneth Progenitor)[14]. The analysis of these data suggested no significant difference in the average level of IL-17RA expression over the course of Paneth cell differentiation, while IL-17RC expression decreased as Paneth cells matured (Fig. 4A). A more detailed analysis, however, demonstrated unique subsets of Paneth progenitors characterized by intermediate levels of Lyz1 and high expression of IL-17RA (Fig. 4B) or IL-17RC (Fig. 4C), consistent with our previous results. Utilizing Paneth^{YFP} (*Defa6-cre;YFP*) mice, we were able to show two distinct Paneth cell populations. The high YFP-positive cells represent matured Paneth cells, and cells expressing low levels of YFP mark Paneth progenitors (Fig. 4D). RT-qPCR analysis of these two populations was consistent with previous results (Fig. 4B, C), demonstrating that low YFP expressing Paneth cells expressed higher levels of *Il17rc*, *Il17ra*, and *Olfm4* (a marker for stemness) (Fig. 4E). Interestingly, we analyzed a previously published single-cell RNA sequencing data (PMID: 29887318) which showed that *Il17rc* and *Il17ra* are upregulated in Paneth cells after irradiation (Fig. 4F)[10]. Taken together, we show that Paneth progenitors, a subset of Paneth cells, express high levels of *Il17ra, Il17rc* and stem cell markers. Furthermore, post irradiation Paneth cells express higher levels of *Il17ra* and *Il17rc*.

IL-17RA signaling promotes Paneth cell stemness after irradiation injury

To better understand the mechanism by which Paneth cells participate in the regeneration of the intestinal crypt after irradiation-induced injury, we generated and validated Paneth cell lineage tracer mice (*Defa6-cre;mT/mG*). All Paneth cells and their lineage in these mice express GFP, while all other cells express RFP. Consistent with published literature[9,10], we were able to show that Paneth cells gain stemness post-irradiation, as revealed by the appearance and counting of ribbons of GFP^{+} cells in the villus 5 days post irradiation (Fig. 5A). Immunofluorescence staining for GFP and MUC2 (goblet cell-specific

https://doi.org/10.1038/s41467-026-70479-z

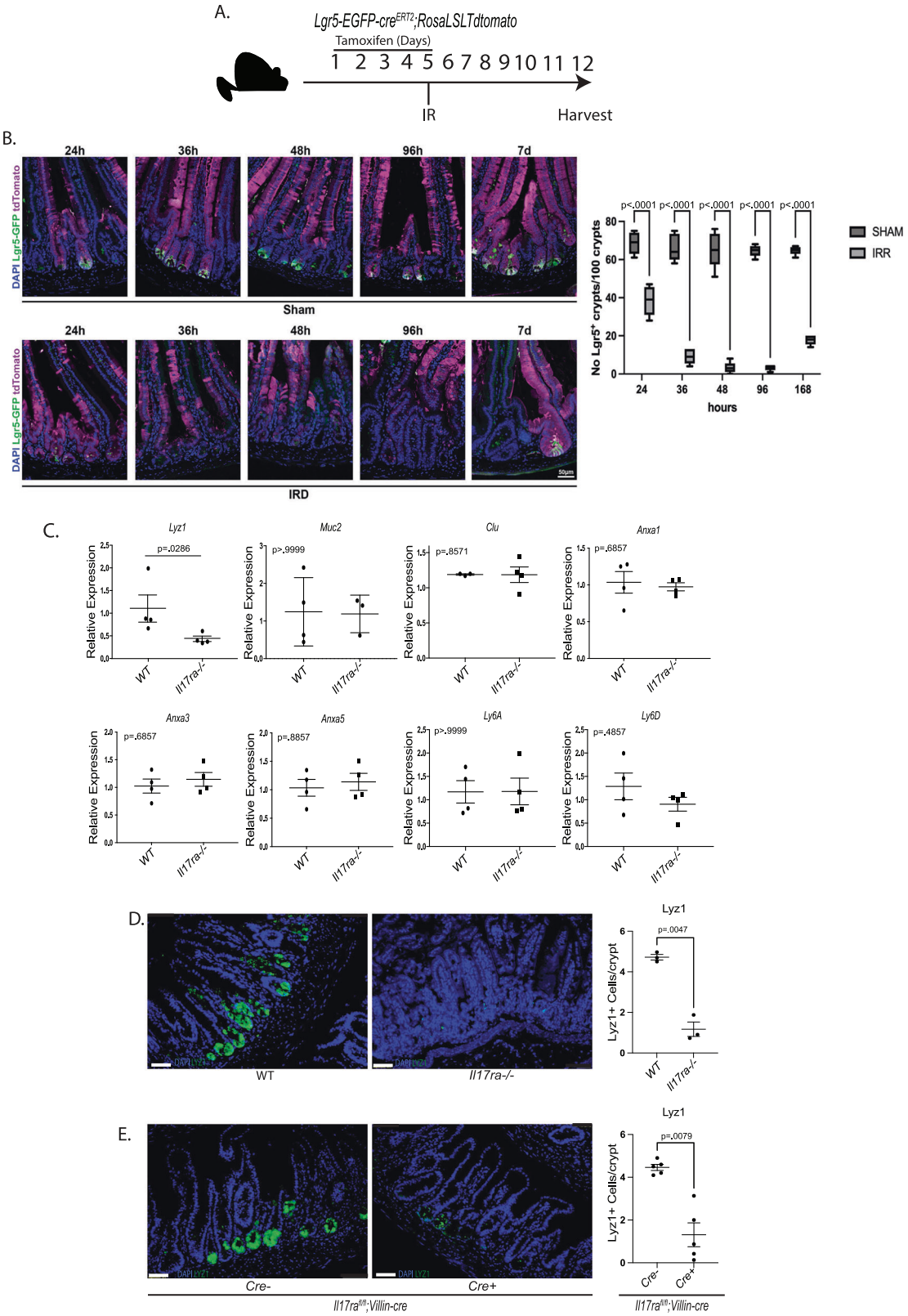

marker) or DCLK1 (Tuft cell marker) or ChGA (enteroendocrine cell marker), or I-FABP (enterocyte cell marker) in these mice showed co-staining of GFP and these distinct cell markers, which supports the assertion that Paneth cells can dedifferentiate and repair/regenerate the intestinal crypt (Fig. 5A and Supplementary Fig. S3A, respectively). Small intestinal crypt from non-irradiated *Defa6-cre;mT/mG* mice forms a viable organoid(Fig. 5B top **panel**). We next sorted GFP$^+$CD24$^+$ Paneth cells from non-irradiated and irradiated *Defa6-cre;mT/mG* mice. Non-irradiated sorted GFP$^+$CD24$^+$ Paneth cells do not form organoid. Green organoids (indicating organoids arising from Paneth cell lineage) only grew from Paneth cells sorted from irradiated mice (Fig. 5B **bottom panel**). To confirm the importance of IL-17A signaling in modulating Paneth cell stemness, we injected *Defa6-cre;mT/mG* mice with anti-IL-17A or IgG antibody on day 0 and day 2 post irradiation

Fig. 2 | LGR5 stem cells ablated after irradiation induced injury. A Schematic depicting the tamoxifen injection and irradiation procedure of *Lgr5-EGFP-cre^{ERT2};RosaLSLTdtomato* mice. **B** Representative immunofluorescent images depicting loss of LGR5 stem cells after irradiation as compared to sham treatment from the ilea of *Lgr5-EGFP-cre^{ERT2};RosaLSLTdtomato* mice (left). Quantification of images (right). A box plot defined as follows: center: median, lower bound: 25th percentile, upper bound: 75th percentile, lower whisker: extends to minima, upper whisker: extends to maxima. Mice were 8–10 weeks old. $N = 50$. **C** RT-qPCR analysis depicting *Lyz1, Muc2, Clu, Anxa1, Anxa3, Anxa5* from *Il17ra^{KO}* mice 3 days post irradiation and *Ly6a*, and *Ly6d* from *Il17ra^{KO}* mice 5 days post irradiation. Mice were 6.6, 13 and 14 weeks old. $N = 8$. **D** Representative immunofluorescent images depicting Lyz1 (green) and DAPI (blue) from the terminal ilea of wild type and *Il17ra^{KO}* mice 5 days after irradiation (scale bar = 50 µm) (left) and quantification (right). Mice were 13 and 14 weeks old. $N = 6$. **E** Representative immunofluorescent images depicting Lyz1 (green) and DAPI (blue) from the terminal ilea of *Il17ra$^{fl/fl}$;Villin-cre +/−* mice 5 days after irradiation (scale bar = 50 µm) (left) and quantification (right). Mice were 7.9 and 14.6 weeks old. $N = 10$. N = number of biologically independent mice. Figure 2B includes at least 3 mice in each group. Figures 2A, B are generated from 3 experiments and Fig. 2D, E are generated from 2 experiments. Figure 2B was analyzed via two-way ANOVA, and Fig. 2D was analyzed via Welch's T-test. Data are presented as ± SEM on relevant graphs. (Mann-Whitney test, Two-tailed, two-way ANOVA, and Welch's T-test, Two-tailed).

(Fig. 5C). We then counted the number of GFP$^+$ cells in the base of the crypt and in the villi between the two treatment groups 5 days post irradiation. We also counted the number of GFP+ clones, which we define as at least 4 GFP + cells in a row, in the villi between the two treatment groups 5 days post-irradiation. The results showed decreased GFP$^+$ cells and clones in the villi of mice treated with anti-IL-17A as compared to IgG-treated mice (Fig. 5D). Furthermore, there was decreased crypt/villi length indicating structural damage in the terminal ilea of mice treated with anti-IL-17A compared to IgG treated mice (Fig. 5E). We also observed reduced proliferation in the ileum of mice treated with anti-IL-17A as compared to IgG-treated mice(Fig. 5F). This result demonstrates a strong connection between IL-17A signaling and Paneth cells ability to dedifferentiate and repair the intestinal crypt after radiation injury. We then established an organoid irradiation and regeneration model and identified that 6 Gy is an optimal dose of irradiation (Supplementary Fig. S3B). Prior literature has also shown that doses lower than 6 Gy show minimal effects on organoid growth, while at 6 Gy, the initial loss of organoid budding was followed by renewed organoid regeneration[36]. To confirm the importance of IL-17A in the regeneration of the intestinal epithelium, we supplied external recombinant IL-17A to organoids grown from *Defa6-cre;mT/mG* mice post-irradiation and observed increased GFP+ cells after IL-17A treatment (Fig. 5G, H). We have previously reported that IL-17A signaling on ISCs promotes secretory lineage commitment[13]. Thus, the increased GFP+ cells we observe after IL-17A treatment may be increased amounts of mature Paneth cells or stem-like Paneth cells. To confirm the presence of stem-like Paneth cells, we passaged these organoids and observed if any fully green organoids grew. Interestingly, when these organoids were passaged, we saw a higher percentage of fully green organoids from the wells that were treated with IL-17A, indicating that IL-17A may directly increase Paneth cell stemness after irradiation (Fig. 5I). Since IL-25 and IL-17C also signal through IL-17RA, we tested whether recombinant IL-25 or IL-17C can induce green organoids after irradiation. Our results showed no significant increase in green organoid development from passaged *Defa6-cre;mT/mG* mice post-irradiation after IL-25 or IL-17C treatment (Supplementary Fig. S3C). We then stained the IL-17A treated green organoids for MUC2 and ChGA. MUC2 marks terminally differentiated goblet cells while ChGA marks terminally differentiated enteroendocrine cells. Since the staining revealed that these green organoids were composed of both GFP + /MUC2 + double-positive cells and GFP + /ChGA + double-positive cells, we can ascertain that these green organoids arise from Paneth cells and are mature organoids composed of terminally differentiated epithelial cells (Fig. 5J). Collectively, our data show that IL-17A promotes Paneth cell dedifferentiation.

Overexpression of *ADAM17* rescued intestinal regeneration defect in *Il17ra$^{fl/fl}$;Defa6-cre+* mice after radiation-induced injury independent of EGFR ligands

We next investigated mechanisms of IL-17A-induced Paneth cell stem-like properties. We performed RT-qPCR analysis in the terminal ileum of *Il17ra$^{fl/fl}$;Defa6-cre* mice for a range of genes involved in tissue regeneration pathways. These genes were selected because epithelial regeneration has been shown to be mediated via WNT, ADAM17, and Notch pathways[9,37,38]. Furthermore, the annexin family genes (*Anxa1, Anxa3, Anxa5*), Ly6 family genes (*Ly6a* and *Ly6d*) and YAP family genes (*Yap* and *Hbegf*) are markers for the fetal-like reversion regenerative pathway[39–41]. We showed decreased expression of *Adam17, Dll1*, and *Wnt9b* in *Il17ra$^{fl/fl}$;Defa6-cre +* mice after radiation injury compared to *cre-* mice. Interestingly, *Ly6a* but not *Ly6d, Anxa1, Anxa3, Anxa5, Yap, and Hbegf* expression was increased in the small intestine of *cre+* mice as compared to *cre-* mice (Fig. 6A Supplementary Fig. S4A). The increased expression of *Ly6a* may be occurring as an alternate regenerative mechanism to compensate for the decrease in expression of *Adam17, Dll1*, and *Wnt9b* after injury. The increased ligand expression of *Ly6a* does not appear to result in noticeable downstream effects. We also grew organoids from our Paneth cell lineage tracer mice and irradiated them for 24 h as described prior. Next, we treated these organoids with IL-17A for 4 h and sorted Paneth cells (Fig. 6B Supplementary Fig. S3D). RT-qPCR analysis of the sorted Paneth cells showed that 4 h treatment of IL-17A directly increased the expression of *Adam17*, specifically in Paneth cells (Fig. 6C). ADAM17 is a metalloprotease involved in the proteolysis of ~80 proteins. Loss of ADAM17 has been shown to cause intestinal regenerative defects and is associated with chronic intestinal injury[38,42,43]. Increased degradation of ADAM17 has also been shown to cause hair follicle stem cell exhaustion due to reduced Notch signaling[44]. Hif1α has been shown to promote *Adam17* expression[45,46]. Thus, we explored if the expression of *Hif1α* and its target genes (*Hk2, Slc2a1, Pgk1*) were also reduced in the terminal ileum of irradiated *Il17ra$^{fl/fl}$;Defa6-cre +* mice. No difference in expression was observed (Fig. 6D). Furthermore, RNA sequencing data (PMID: 29887318) also showed no difference in the expression of Hif1α related genes in Paneth cells post irradiation (Fig. 6E)[10]. ADAM17 has also been shown to be modulated via NADPH oxidase 1 (Nox1). Specifically, the stability of ADAM17 has been shown to be mediated through Nox1. Nox1 has been shown to protect ADAM17 from ubiquitin-mediated degradation through direct interactions[47]. Nox1 is also an important producer of intestinal epithelial ROS. Depletion of Nox1 significantly reduces intestinal epithelial ROS production[48]. Oxidative stress and redox agents have been shown to activate ADAM17 and induce shedding of ADAM17 targets[49,50]. Thus, we explored if Nox1 may play a role in our observations. Expression of *Nox1* was reduced in both naïve and irradiated *Il17ra$^{fl/fl}$;Defa6-cre +* as compared to *cre-* mice, while expression patterns of other proliferative pathway genes remained unchanged between naïve *Il17ra$^{fl/fl}$;Defa6-cre +* and *cre-* mice (Supplementary Fig. S1K and Fig. 6F). Furthermore, immunohistochemistry (IHC) staining for Nox1 showed decreased Nox1 protein amounts in *Il17ra$^{fl/fl}$;Defa6-cre +* as compared to *cre-* post irradiation (Supplementary Fig. S4B). RT-qPCR analysis of the sorted Paneth cells showed that 4 h treatment of IL-17A also directly increased expression of *Nox1* specifically in Paneth cells (Fig. 6G). Analysis of a previously published single-cell RNA sequencing data (PMID: 29887318) also showed increased expression of *Adam17, Nox1, and Olfm4* in Paneth cells post irradiation (Fig. 6H)[10]. Since Nox1 is a major producer of ROS,

https://doi.org/10.1038/s41467-026-70479-z

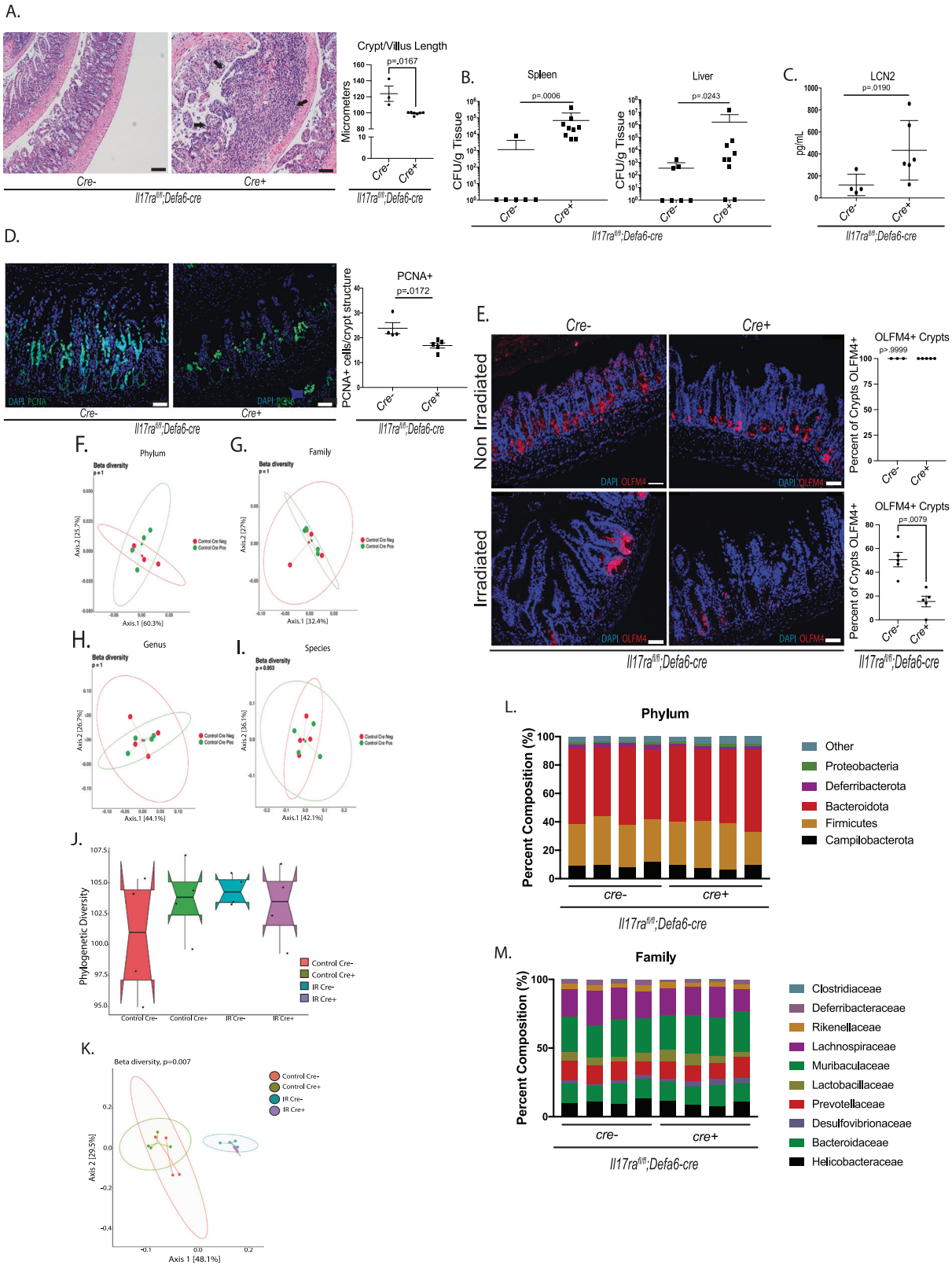

we next show that exogenous redox agents such as H_2O_2 is able to directly induce ADAM17 activity (Fig. 6I). To confirm the importance of ROS in modulating Paneth cell stemness, we gave Paneth cell lineage tracer mice 4% n-acetylcysteine (NAC) in their drinking water after irradiation[51]. NAC is an antioxidant, which has been shown to be readily metabolized within the small intestine[52]. Mice were kept on 4% NAC water until euthanasia, 5 days post irradiation (Fig. 6J). We then quantified the number of GFP^+ cells in the crypt and villi between the two treatment groups. The results showed decreased GFP^+ cells and clones in the villi of mice given on 4% NAC water as compared to mice given untreated water (Fig. 6K). We also observed a trend towards decreased ADAM17 activity in the ileum of mice given on 4% NAC water as compared to mice given untreated water (Supplementary Fig. S4C).

Fig. 3 | IL-17RA signaling to Paneth cells helps maintain intestinal integrity after irradiation induced injury. A Representative images of hematoxylin and eosin staining of terminal ilea in *Il17ra*$^{fl/fl}$*;Defa6-cre* + /− mice 3 days after irradiation (scale bar = 100 µm) (left). Arrows represent areas of damage. Quantification of crypt lengths (right). Mice were 6.9 and 10.6 weeks old. *N* = 10. **B** Splenic and hepatic bacterial dissemination in *Il17ra*$^{fl/fl}$*;Defa6-cre* + /− mice 5 days after irradiation. Mice were 8.0, 8.1 and 10.6 weeks old. *N* = 16. **C** Amounts of lipocalin in cecal content of 5 day post irradiated *Il17ra*$^{fl/fl}$*;Defa6-cre* + /− mice measured via ELISA. Mice were 8.1 and 10.4 weeks old. *N* = 10. **D** Representative immunofluorescent images depicting PCNA (green) and DAPI (blue) from the ileum of *Il17ra*$^{fl/fl}$*;Defa6-cre* + /− mice 3 days after irradiation (scale bar = 50 µm) (left) and quantification (right). Mice were 6.9, 8.9 and 10.6 weeks old. *N* = 9. **E** Representative immunofluorescent images depicting OLFM4 (red) and DAPI (blue) from the ileum of non- irradiated (top) and 5 days post-irradiated (bottom) *Il17ra*$^{fl/fl}$*;Defa6-cre* + /- mice (scale bar = 50 µm) (left) and quantification (right). Mice were 6.7, 10, and 11.6 weeks old. *E* = 8. **F**–**I** Phylum, family, genus, and species beta diversity between non-irradiated *Il17ra*$^{fl/fl}$*;Defa6-cre* + /− mice. Mice were 6.4 weeks old. *N* = 16. **J** Phylogenetic diversity between non-irradiated and 5 day post irradiated *Il17ra*$^{fl/fl}$*;Defa6-cre* + /− mice. Mice were 6.4 and 7.1 weeks old. Box plot defined as follows: centre: median, lower bound: 25th percentile, upper bound: 75th percentile, lower whisker: extends to minima, upper whisker: extends to maxima. *N* = 16. **K** Beta diversity between non-irradiated and 5 day post irradiated *Il17ra*$^{fl/fl}$*;Defa6-cre* + /- mice. Mice were 6.4 and 7.1 weeks old. *N* = 16. **L**, **M** Terminal ileum cecal contents of cohoused littermate, irradiated, *Il17ra*$^{fl/fl}$*;Defa6-cre* + /− mice were analyzed for commensal diversity at the phyla (top) and selected family (bottom) levels via 16 S microbial sequencing. Mice were 7.1 weeks old. *N* = 16. *N* = number of biologically independent mice. Figure 3A, C, E data is generated from 2 independent experiments. Figure 3B, D data are generated from 3 independent experiments. Data are presented as ± SEM on relevant graphs. (Mann-Whitney test, Two-tailed).

Next, to study the role of ADAM17 in our observations, we utilized an ADAM17 adenovirus (Ad-Adam17) to overexpress *ADAM17* (Fig. 6L Supplementary Fig. S4D). Overexpression of *ADAM17* rescued *Il17ra*$^{fl/fl}$*;Defa6-cre* + mice from structural damage as well, while not affecting Paneth cell number (Fig. 6M & Figure S4E). Increased cellular proliferation was observed in the ileum of *Il17ra*$^{fl/fl}$*;Defa6-cre* + after overexpression of *ADAM17* (Fig. 6N). Overexpression of *ADAM17* in *Il17ra*$^{fl/fl}$*;Defa6-cre* + showed reduced bacterial burden in their liver post irradiation injury (Fig. 6O). This was coupled with a trend towards decreased cecal LCN2 in these mice as well (Supplementary Fig. S4F). Collectively, our data show that ADAM17 is required for intestinal epithelial regeneration.

ADAM17 expression in Paneth cells contributes to intestinal regeneration after radiation-induced injury

We confirmed that both naïve and irradiated Paneth cells express ADAM17 by immunostaining the terminal ileum of control and irradiated *Defa6-cre;mT/mG* mice (Supplementary Fig. S5A, S5B). We next generated Paneth (*Defa6*) cell-specific *Adam17* knockout mice. Reduced staining of ADAM17 in Paneth cells in the ilea of *Adam17*$^{fl/fl}$*;Defa6-cre* + mice confirmed the specificity of the deletion (Supplementary Fig. S6). We then irradiated *Adam17*$^{fl/fl}$*;Defa6-cre* + /- mice. Five days after irradiation *Adam17*$^{fl/fl}$*;Defa6-cre*+ mice had greater structural damage than their *cre*- counterparts (Fig. 7A). We also observed increased cecal LCN2 and increased hepatic and splenic bacterial dissemination in irradiated *cre*+ mice (Fig. 7B, C). Irradiated *cre* + mice also had reduced proliferation as compared to their *cre*- counterparts (Fig. 7D). To determine whether ADAM17 expression on Paneth cells was important for Paneth cell-specific proliferation, we stained irradiated *Adam17*$^{fl/fl}$*;Defa6-cre* + /− mice for PCNA and Lyz1. We saw decreased amounts of proliferating Paneth cells in irradiated *Adam17*$^{fl/fl}$*;Defa6-cre* + mice as compared to *cre*- mice (Fig. 7E). While Paneth cell-specific proliferation was decreased in *Adam17*$^{fl/fl}$*;Defa6-cre* +, overall proliferation remains was not effected. The intestinal epithelium has been shown to have high plasticity, where a wide variety of epithelial cells can dedifferentiate to regenerate the epithelium in the absence of ISCs[27,53]. Thus, we believe if Paneth cell dedifferentiation is inhibited, other cell types would then help regenerate the intestine. While RT-qPCR analysis of regenerative markers within the terminal ileum yielded no significant differences between irradiated *Adam17*$^{fl/fl}$*;Defa6-cre* + /− mice, we did see a strong trend towards decreased *Nox1* expression in *Adam17*$^{fl/fl}$*;Defa6-cre* + mice (Fig. 7F). To validate these finding, we stained for Nox1 in the ileum of irradiated *Adam17*$^{fl/fl}$*;Defa6-cre* + /− mice. Indeed, we saw decreased Nox1+ crypts/villi in *Adam17*$^{fl/fl}$*;Defa6-cre*+ mice as compared to *cre*- mice (Fig. 7G). Nox1 has been show to stabilize and promote ADAM17 activation, which in turn can then activate the EGFR-ERK1/2 pathway.[47,54,55]. The EGFR-ERK1/2 pathway modulates ATF-1, which has been shown to promote NOX1 signaling[56]. Thus, Adam17 expression and Nox1 expression may result from a positive feedback loop and rely upon each other. We next wanted to determine if Paneth cell specific ADAM17 played a role in intestinal epithelial barrier integrity. First, we stained for ZO-1, a common epithelial cell tight junction protein, in the terminal ilea of irradiated *Adam17*$^{fl/fl}$*;Defa6-cre* + and *cre*- mice. We then looked at expression levels of two other tight junction proteins, *Ocln* and *Cldn4*, in the ilea of these mice. There was no difference in gap junction protein amounts or expression between *Adam17*$^{fl/fl}$*;Defa6-cre* + and *cre*- mice post irradiation (Fig. 7H–I). Taken together, these results show that Paneth cell-specific ADAM17 signaling is vital in limiting damage in response to irradiation via promoting cellular proliferation rather than modulating gut barrier proteins.

Discussion

IL-17RA has been shown to help maintain intestinal barrier integrity and promote gut microbiota homeostasis[22–25]. Furthermore, we have recently published work depicting the importance of IL-17A in promoting secretory lineage commitment via its signaling on Lgr5^{+} stem cells[13]. In this study, we reported that Paneth cell-specific IL-17RA signaling is dispensable during Atoh1 mediated secretory cell regulation during dextran sodium sulfate (DSS) induced colitis. It is important to note that DSS induced injury occurs mainly in the colon, while small intestinal injuries are less severe[57]. Irradiation injury does not have the same limits and can cause extensive small intestinal injury, as seen in patients receiving radiation treatment[58]. Furthermore, chemical induced injuries, such as DSS, and irradiation induced injuries have distinct damage inducing mechanisms, and thus may recover via different pathways[59]. While the significance of IL-17RA signaling within the gut has been established, there is much work needed to determine its importance in signaling to specific intestinal epithelial cell types. Our findings support previous observations, which state that IL-17RA signaling to Paneth cells promotes an anti-inflammatory environment within the ileum[60]. Furthermore, our findings revealed a critical function of IL-17RA promoting stemness in Paneth cells after injury. Our results from germline global IL-17RA (*Il17ra*^{KO}) and intestinal epithelial-specific (*Il17ra*$^{fl/fl}$*;Villin-cre* +) knockout mice showed increased bacterial dissemination to liver and spleen as compared to their WT and *cre*- counterparts after radiation-induced injury. This was coupled with increased inflammation and structural damage.

While the phenotype seen in irradiated *Il17ra*^{KO} and *Il17ra*$^{fl/fl}$*;Villin-cre* + was recapitulated in Paneth cell-specific (*Il17ra*$^{fl/fl}$*;Defa6-cre)* mice, it is important to note that only a small subset of Paneth progenitors express high levels of IL-17RA. We believe these Paneth progenitor cells drive Paneth cell- specific regeneration post irradiation injury rather than mature Paneth cells. Paneth progenitor cells have a unique expression profile (high *Il17ra/rc* and *Olfm4*), which allows them to be primed for rapid dedifferentiation in response to injury and increased IL-17A signaling. Furthermore, other cell types have also been shown to

https://doi.org/10.1038/s41467-026-70479-z

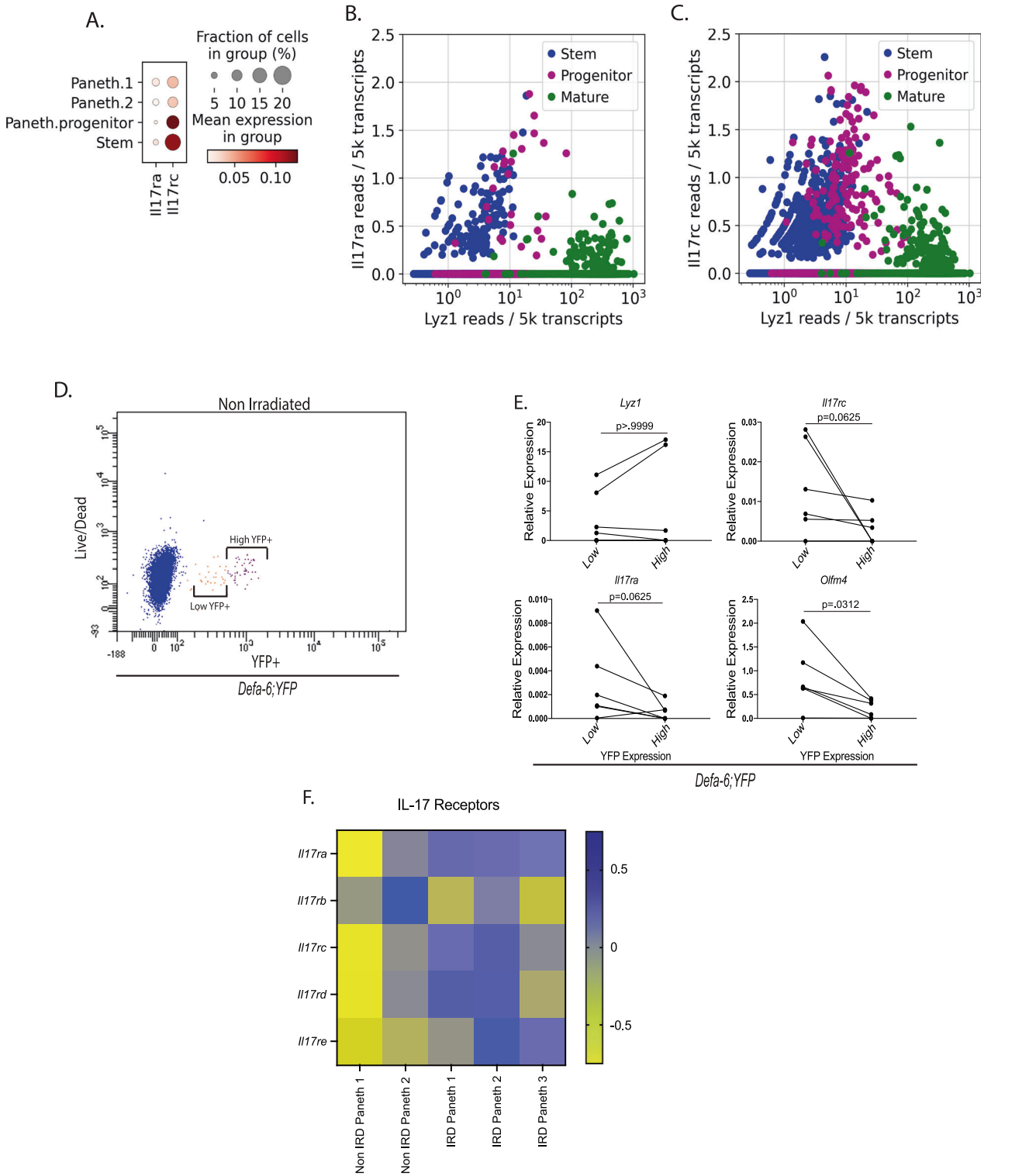

Fig. 4 | Highest expression of IL-17RA is on Paneth progenitors. A The expression pattern *of Il17ra and Il17rc* genes on Paneth 1, Paneth 2, Paneth progenitors and intestinal stem cells (PMID: 29144463). **B** Scatter plot expression *of Il17ra* and *Lyz1* on mature Paneth cells, Paneth progenitors, and intestinal stem cells (PMID: 29144463). **C** Scatter plot expression *of Il17rc* and *Lyz1* on mature Paneth cells, Paneth progenitors, and intestinal stem cells (PMID: 29144463). **D** Representative flow cytometry plot from *Paneth*^{YFP} mice depicting high and low YFP expression. **E** RT-qPCR analysis of *Lyz1, Il17rc, Il17ra, and Olfm4* between low YFP and high YFP populations of Paneth cells from naïve Paneth^{YFP} mice. Mice were 7.6, 9.9, and 3.3 weeks old. $N = 6$. **F** Single-cell RNA sequencing heat map data depicting expression of IL-17 receptor family genes from non-irradiated and irradiated Paneth cells (PMID: 29887318). N = number of biologically independent mice. Figure 4D, E are generated from 3 independent experiments. (Wilcox paired test, Two-tailed).

https://doi.org/10.1038/s41467-026-70479-z

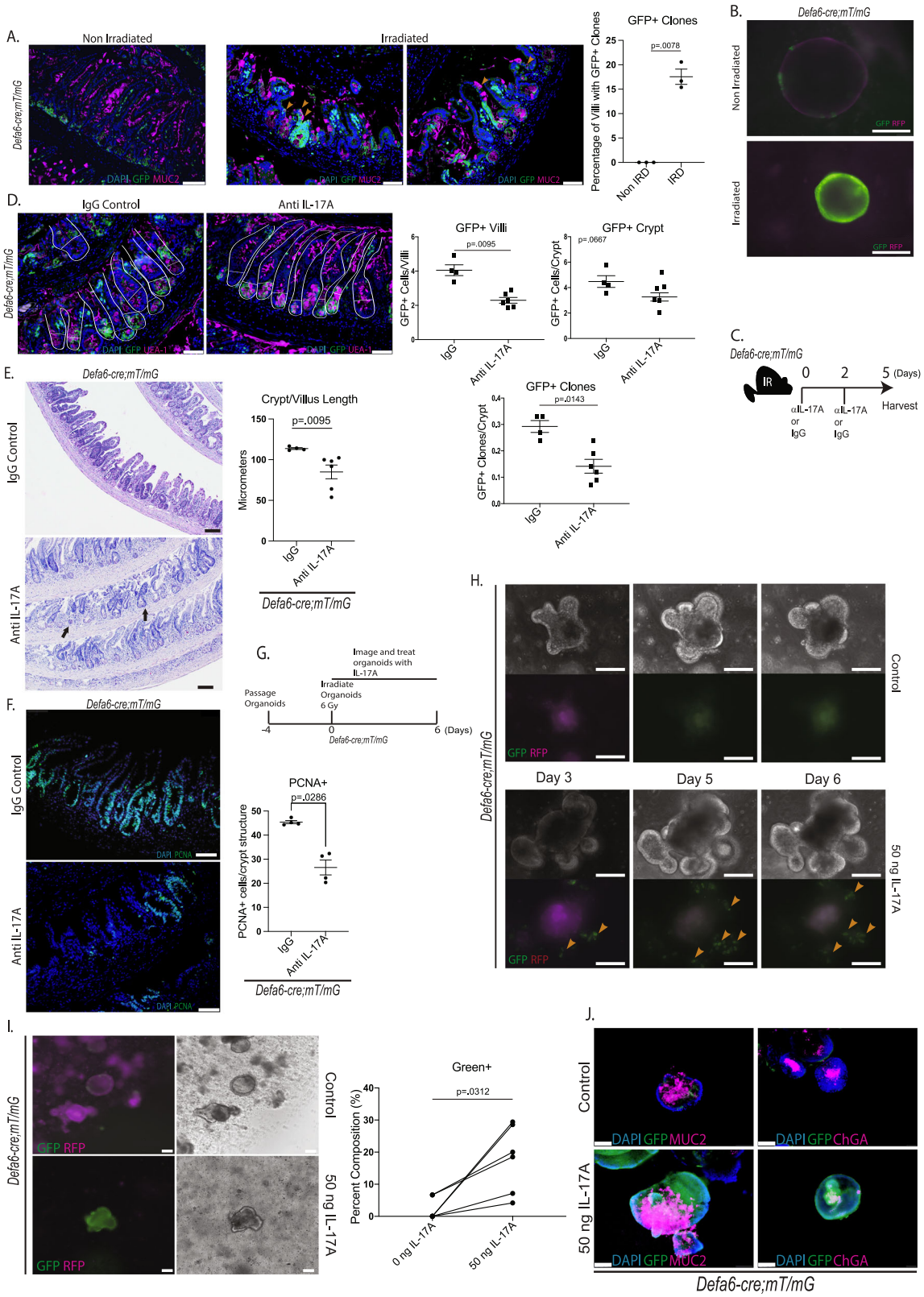

regenerate the intestinal epithelium after injury. It has long been understood that there are two predominant populations of ISCs: Lgr5$^+$ stem cells and reserve stem cells. Lgr5$^+$ stem cells are the population of ISCs constitutively replicating and replenishing the epithelium via canonical WNT signaling pathways[61]. Conversely, reserve stem cells are not actively proliferating, are insensitive to WNT signaling, and are considered quiescent. However, after injury and loss of Lgr5$^+$ stem cells, Bmi1$^+$ stem cells expand rapidly and help repopulate the intestinal epithelium[62]. *Clu*$^+$ cells are another ISC rare under homeostatic conditions but undergo a YAP1-mediated expansion and can help replenish the intestinal epithelium[11]. Recently, progenitor cells located in the isthmus region have also been shown to promote intestinal regeneration[53,63]. Moreover, terminally differentiated cells such as enteroendocrine cells have also been shown to be able to

Fig. 5 | IL-17RA signaling to Paneth cells promotes Paneth cell stemness after irradiation. A Ileum of non-irradiated and irradiated *Defa6-cre;mT/mG* mice (scale bar = 50 µm) (GFP = green), (MUC2 = magenta), (DAPI = blue). Arrows represent areas of GFP + /MUC2 + co-staining. Mice were 9, 14.3, and 11 weeks old. *N* = 6. **B** Organoids cultured from non-irradiated small intestinal crypt and irradiated sorted GFP$^+$CD24$^+$ cells from *Defa6-cre;mT/mG* mice (green = Paneth cell lineage) (Magenta = non-Paneth cell lineage) (scale bar = 300 µm). **C** Experimental schematic. **D** Ileum of irradiated *Defa6-cre;mT/mG* mice treated with isotype or anti-IL-17A (250 µg/mouse) (scale bar = 50 µm) (GFP = green), (UEA-1 = magenta) and (DAPI = blue). GFP + clones = 4 cells in a row. Mice were 7.3, 13.3, and 10 weeks old. *N* = 10. **E** Hematoxylin and eosin staining from the terminal ileum of irradiated *Defa6-cre;mT/mG* mice treated with IgG or anti-IL-17A (250µg/mouse) (scale bar = 100 µm). Mice were 7.3, 13.3, and 10 weeks old. *N* = 10. **F** Ileum of irradiated *Defa6-cre;mT/mG* mice treated with IgG or anti-IL-17A (250µg/mouse) (scale bar = 50 µm) (PCNA = green) and (DAPI = blue). Mice were 7.3, 13.3, and 10 weeks old. *N* = 8. **G** Experimental schematic. **H** Irradiated organoids cultured from *Defa6-cre;mT/mG* mice 3, 5, and 6 days post irradiation (green = Paneth cell lineage) (magenta = non-Paneth cell lineage) (scale bar = 300 µm). Arrows indicate GFP+ cells. **I** Organoids passaged from those shown in Fig. 5H (green = Paneth cell lineage) (magenta = non-Paneth cell lineage) (scale bar = 300 µm) (left). Quantification of the percent composition of green organoids out of total organoids (right). *N* = 6. **J** Green organoids stained for Muc2 and ChGA (blue = DAPI) (green = Paneth cell lineage) (magenta = Muc2 or ChGA) (scale bar = 100 µm). *N* = number of biologically independent mice. Figure 5B, H are representative of 3 mice. Figure 5D, E, F, J = 2 independent experiments. Figure 5A, B, H, I = 3 independent experiments. Data are presented as ± SEM on relevant graphs. (Mann-Whitney test, Two-tailed and Wilcox paired test, Two-tailed).

dedifferentiate and replenish the intestinal crypt after injury[27]. Whether IL-17RA signaling plays a role in these other cell types has yet to be studied. While we assert that Paneth cells play an important role in replenishing the intestinal epithelium post injury, we believe they work in synergy with other cell types to fully replenish the intestinal epithelium.

Recently, it has been shown that Paneth cells can gain stemness and replenish the intestinal crypt in the absence of Lgr5$^+$ stem cells. Multiple pathways, including Notch signaling and a stem cell factor/c-Kit axis, have been implicated in this phenomenon[9,10,12]. While we also showed that Paneth cells can dedifferentiate and replenish the intestinal crypt, we characterized an IL-17RA-Adam17 dependent mechanism. We show that *Adam17* expression is dependent on IL-17RA signaling in Paneth cells after irradiation induced injury. Furthermore, upregulation of *ADAM17* can protect against irradiation-induced injury in *Il17ra$^{fl/fl}$;Defa6-cre* + mice. ADAM17 is a metalloprotease that cleaves a wide variety of proteins with various downstream effects[64]. Hif1α has been shown to be induced by IL-17A and upregulate ADAM17 in certain situations[45,57]. While we don't see any changes in Hif1α expression or its related genes, ADAM17 is also regulated in other ways. We show that IL-17RA signaling on Paneth cells directly induces *Nox1* expression. Nox1 can promote ADAM17 activity through multiple pathways. Nox1 is an important producer of ROS, while oxidative stress and redox reagents also promote ADAM17 activity[49,50]. Nox1 can also stabilize ADAM17 independent of ROS. Nox1 can directly interact with ADAM17 and protect it from ubiquitination and subsequent degradation[47]. ADAM17 sheds ~80 proteins with various downstream signaling effects[65]. With such a large shedome, it is probable that rather than having one central cleavage product, IL-17RA may promote the shedding of a distinct group of cleavage products, promoting intestinal regeneration. Increased degradation of ADAM17 has also been shown to cause hair follicle stem cell exhaustion due to reduced Notch signaling[44]. ADAM17 has been proven to be clinically relevant as well. Pediatric patients with ADAM17 homozygous mutations have multi-organ developmental defects associated with pediatric enteropathy[38]. We expand upon these findings to show that ADAM17 signaling, specifically to Paneth cells, is essential for protection against radiation-induced injury. It would be interesting to elucidate which ADAM17 product(s) is directly correlated to IL-17RA signaling within Paneth cells.

Irradiation therapy is commonly used to help treat patients suffering from various forms of cancer. Unfortunately, acute intestinal injury is a major side effect of irradiation therapy. These side effects can cause morbidity and may also reduce the effectiveness of the treatment[66]. Our data indicates that IL-17RA signaling to Paneth cells helps protect from irradiation induced intestinal injury. More specifically, we show that Paneth cell mediated intestinal regeneration may be driven by IL-17RA-modulated ADAM17. This study helps highlight a mechanism by which Paneth cells can dedifferentiate and why IL-17A treatment may be a beneficial therapy for patients suffering from IBD and the side effects of irradiation therapy.

Methods

Study design

Animal studies were conducted with the approval and under all relevant ethical regulations of Stony Brook University's Institutional Animal Care and Use Committee (IACUC protocol number 968871). The objective of this study was to determine the significance of IL-17RA signaling to Paneth cells in response to irradiation induced injury. Various genetically modified mice were utilized for this study. An irradiation-based injury model was utilized to study morphological, immunological, and regenerative changes within the small intestine. Sample sizes and replicates used were based on prior literature and experience with various tissue *Il17ra* knockout mice[12,13]. Euthanasia time points were determined based on prior literature[33].

Mice

C57BL/6 (WT), *Villin-Cre* (C57BL/6 background), *Gt(ROSA)26Sor$^{tm1(EYFP)Cos}$/J* (C57BL/6 background) and *ROSA$^{mT/mG}$* (C57BL/6 background) mice were purchased from The Jackson Laboratory. *Il17RA^{KO}* mice were obtained from Dr. Jay Kolls, Tulane University. *Defa6-Cre* mice were obtained from Dr. Richard Blumberg, Brigham and Women's Hospital, Harvard. *Lgr5-EGFP-cre^{ERT2}*, *Lgr5-EGFP-cre^{ERT2};RosaLSLTdtomato* and *Villin-cre^{ERT2}* mice were obtained from Dr. Vincent W. Yang, Stony Brook University. *Adam17$^{fl/fl}$* mice were obtained from Dr. Rebecca K. Martin, Virginia Commonwealth University. Generation and characterization of IL-17-Floxed (*Il17ra$^{fl/fl}$*) mice were performed as previously described[25]. *Il17ra$^{fl/fl}$* mice were bred with *Villin-Cre* or *Defa6-Cre* to develop entire gut epithelium and Paneth cell-specific IL-17RA knockout mice. *Defa6-Cre* mice were bred with *Gt(ROSA)26Sor$^{tm1(EYFP)Cos}$/J* or *ROSA$^{mT/mG}$* mice to develop Paneth^{YFP} and Paneth cell lineage tracing mice, respectively. *Adam17$^{fl/fl}$* mice were bred with *Defa6-Cre* mice to develop Paneth cell-specific ADAM17 knockout mice. Mice of both genders were used for all experiments unless indicated in the figures. Mice ages for each experiment are provided in the figure legends. Littermate controls were used for experiments, thus all *cre-* and *cre+* mice were age matched. Sex was not considered in this study design and analysis as it was not relevant to our findings. All mice were housed in specific pathogen-free conditions at Stony Brook University, Stony Brook, NY. All animal studies were conducted with the approval of Stony Brook University's Institutional Animal Care and Use Committee.

Animal treatment

Anti-17A or IgG control (250µg/mouse) was administered intraperitoneally to mice on the same day of irradiation and 2 days post irradiation for select experiments. Mice were given 4% n-acetylcysteine in

https://doi.org/10.1038/s41467-026-70479-z

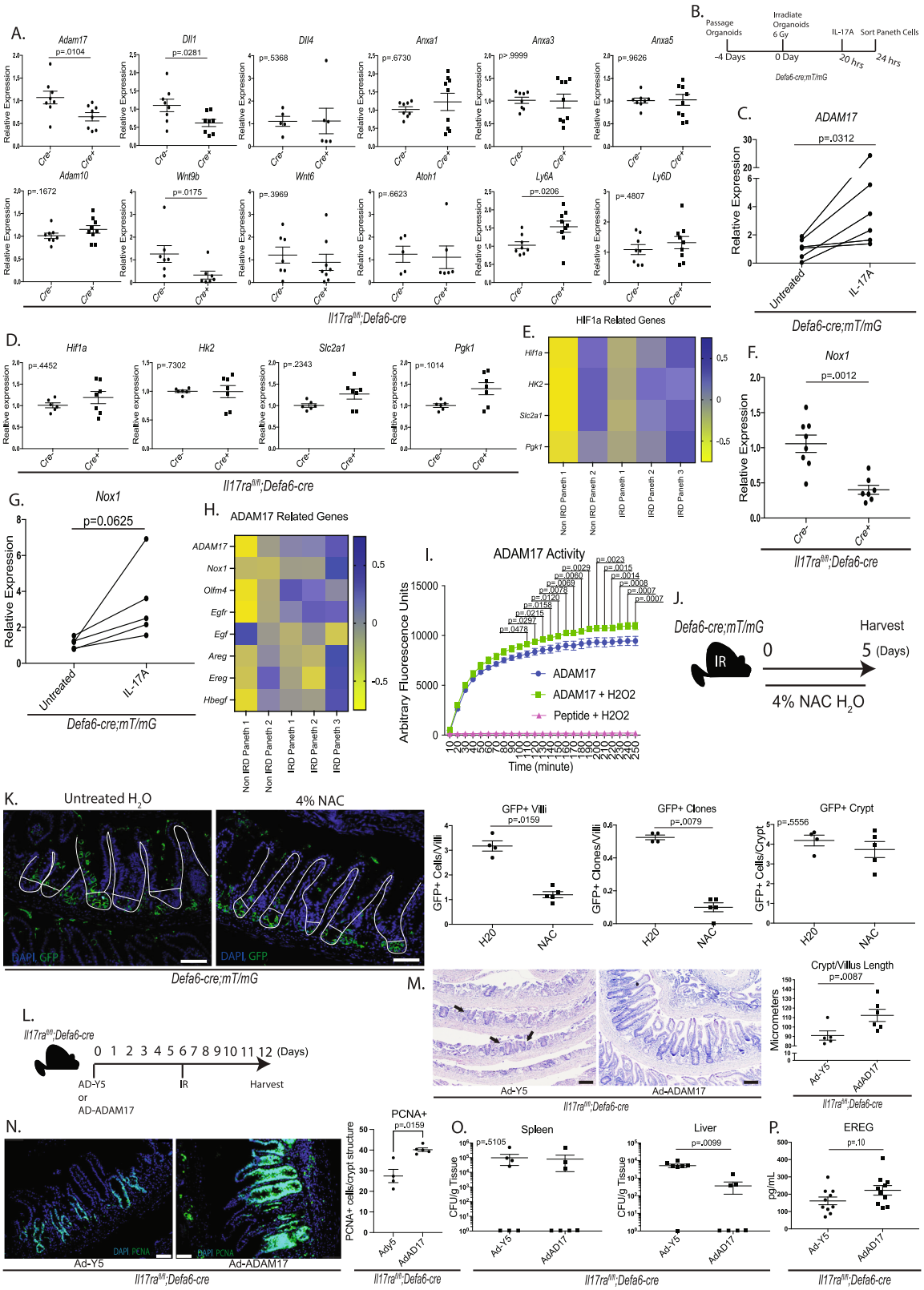

their drinking water directly after irradiation continuously until euthanasia on day 5 post irradiation for select experiments.

Cell lines and organoid cultures

L-WRN cell line was obtained from Dr. Thaddeus Stappenbeck, Washington University. The HEK-293 cell line was obtained from Dr. Vincent W. Yang, Stony Brook University.

Irradiation treatment

Mice were irradiated at 12 Gy in a gamma cell irradiator (GammaCell 40; AEC Ltd). WT (C57BL/6) and *Il17ra*^{KO} mice bedding was mixed 1 week prior to gamma-irradiation to help ensure mixing of gut microbiota. Mice were euthanized at various time points (3 and 5 days) post-irradiation, and tissue was collected for experiments. Organoids were initially irradiated at increasing doses of gamma cell irradiation in

Fig. 6 | Loss of IL-17RA signaling on Paneth cells results in reduced expression of *Adam17* after irradiation. **A** Gene expression from irradiated *Il17ra*$^{fl/fl}$*;Defa6-cre* + /− mice (6.7, 8.1 weeks old); each point represents an independent mouse. **B** Experimental schematic. **C** *Adam17* expression in sorted irradiated Paneth cells after 4 h of IL-17A treatment from *Defa6-cre;mT/mG* organoids. *N* = 6. **D** Gene expression from irradiated *Il17ra*$^{fl/fl}$*;Defa6-cre* + /− mice (6.7, 8.1 weeks old). *N* = 13. **E** Single-cell RNA sequencing of *Hif1a* related genes from non-irradiated and irradiated Paneth cells (PMID: 29887318). **F** Terminal ileal *Nox1* expression from irradiated *Il17ra*$^{fl/fl}$*;Defa6-cre* + /− mice (6.7 < 8.1 weeks old). *N* = 15. **G** *Nox1* expression in sorted irradiated Paneth cells after 4 hours of IL-17A treatment. *N* = 5. **H** Single-cell RNA sequencing expression of Adam17 related genes from non irradiated and irradiated Paneth cells (PMID: 29887318). **I** ADAM17 activity +/- 4 mM H_2O_2. **J** Experimental schematic. **K** Ileum of irradiated *Defa6-cre;mT/mG* mice given water or 4% NAC water (GFP = green) (DAPI = blue) (scale bar = 50 µm). GFP + clones = 4 cells in a row. Mice were 8.3 and 13.4 weeks old. *N* = 9. **L** Experimental schematic. **M** Hematoxylin and eosin staining of terminal ilea in *Il17ra*$^{fl/fl}$*;Defa6-cre* + mice treated with Ad-Y5 or Ad-Adam17 (AdAD17) 5 days after irradiation (scale bar = 100 µm). Mice were 8.9, 14.1 and 15.1 weeks old. *N* = 11. **N** Ileum of *Il17ra*$^{fl/fl}$*;Defa6-cre* + mice treated with Ad-Y5 or AdAD17 5 days after irradiation (PCNA = green) (DAPI = blue) (scale bar = 50 µm). Mice were 8.9, 14.1 and 15.1 weeks old. *N* = 9. **O** Bacterial dissemination in *Il17ra*$^{fl/fl}$*;Defa6-cre* + /− mice treated with Ad-Y5 or AdAD17 5 days after irradiation. Mice were 8.9, 14.1 and 15.1 weeks old. *N* = 14. **P** EREG in the ileum of *Il17ra*$^{fl/fl}$*;Defa6-cre* + /− mice treated with Ad-Y5 or AdAD17 5 days after irradiation. Mice were 8.9, 14.1 and 15.1 weeks old. *N* = 20. *N* = number of biologically independent mice. 6 K, 6 M, 6 N, 6 O = 2 independent experiments. 6 A, 6 C, 6D, 6 F, 6 G, 6 L = 3 independent experiments. Outliers removed via GraphPad Prism (ROUT analysis, Q = 1%) in Fig. 6A. Data are presented as ± SEM on relevant graphs (Mann-Whitney test, Two-tailed and Wilcox paired test, Two-tailed).

a gamma cell irradiator (GammaCell 40; AEC Ltd) to develop our model. Once we confirmed 6 Gy as our optimal dose, all successive organoids were irradiated at 6 Gy. Organoids were then imaged and collected for RT-qPCR, varying days post irradiation (3, 5, 6 days).

Bacterial dissemination

Mice were euthanized 5 days post-irradiation, and their livers and spleens were harvested, weighed, homogenized, and plated on Luria broth (LB) or brain heart infusion (BHI) plates. After 48 hours, colonies were counted. Homogenates were also incubated in an anaerobic chamber (GasPak anaerobic container) for 48 hours and then counted to determine the dissemination of anaerobic bacteria.

Bone marrow transplantation

Wild type (WT) and *Il17ra*^{KO} mice were irradiated at 12 Gy. Non-irradiated WT and *Il17ra*^{KO} mice were euthanized, and bone marrow was extracted from their femurs. Extracted bone marrow was then transplanted into their irradiated counterparts 2 hours post irradiation (1 million cells). Mice were then euthanized 5 days post irradiation and livers and spleens were harvested to measure bacterial dissemination as previously described and the mesenteric lymph node was isolated for flow cytometry to ensure transplantation.

Induction of gene knockouts

To induce the knockout of genes, tamoxifen (1 mg/mouse) was administered intraperitoneally from day 0 to day 5 to *Lgr5-EGFP-cre*^{ERT2}*;RosaLSLTdtomato* mice. On day 5, mice were irradiated and euthanized at multiple time points, and tissues were harvested for bacterial dissemination.

Crypt Isolation

Ileums were harvested and flushed with ice-cold 1x PBS. They were then cut open longitudinally, and Peyer's patches were removed and cut into ~ 2 cm sections. Tissues were then washed in 30 mL of ice-cold 1 x PBS 3 times. Tissues were then incubated in 1x ice-cold PBS supplemented with 3.75 mM EDTA on an orbital rocket (60 rpm) for 30 minat 4 °C. Tissues were then washed twice with 50 mL of 1x ice-cold PBS. Tissues were then moderately shaken in 25 mL of ice-cold 1x PBS and filtered through 70 micron filters to extract crypts. This was repeated three times to maximize crypt accumulation.

Organoid culture

Isolate crypts were pelleted (300 x g) and re-suspended in Matrigel Matrix (Corning) at a concentration of ~ 100 crypts per 30 µL Matrigel Matrix. 24-well plates were then seeded with 30 µL/well of crypt suspension. The seeded plates were then incubated at 37 °C, 5% CO_2 for 15 min to allow for Matrigel polymerization. The polymerized domes were then immersed in 500 µL of enriched organoid growth medium (1:1 mixture of L-WRN and DMEM/F12) containing 1 x penicillin-streptomycin-glutamine (Invitrogen), 1 x B27 (Invitrogen), 1 x N2 (Invitrogen), 50 ng/mL of murine EGF (R&D system), 1 mM of N-acetylcysteine (Sigma-Aldrich), 10 nM of Gastrin-Leu15 (Sigma-Aldrich), 500 nM of A83-01 (Torics), 10 mM of Y-27632 (Sigma-Aldrich) and 10 mM of CHIR99021 (Tocris). After 2 days, enriched organoid growth medium was replaced with supplemented organoid growth medium (no Y-27632 and CHIR99021). Supplemented organoid growth medium was continuously replaced every 2 days. Organoids were treated with IL-17A (50 ng/ml) every 2 days and harvested on day 6 for RT-PCR. Images were taken on days represented in figures with an Olympus CKX41 microscope.

For passaging, organoids were lifted in 500 µL of cell recovery solution and incubated on an orbital shaker for 5 min at room temperature. Organoids were then pelleted (300 g) and incubated in TrypLE Express (Thermo Fisher) for 5 min to make a single cell solution. Cells were then resuspended in Matrigel Matrix and plated in a 24-well plate (30 µL/well). Domes were then resuspended in enriched organoid growth medium and cultured as described above.

RT-qPCR

RNA was extracted from terminal ileum tissues via Trizol-based extraction or from organoids via RNeasy Mini Kit (QIAGEN). RNA was reverse transcribed into cDNA using Bio-Rad iScript kits according to the manufacturer's protocol. RT-PCR was performed by mixing 5 µL of SsoAdvanced Universal Probes Supermix (Bio-Rad) or SsoAdvanced Universal SYBR Green Supermix (Bio-Rad), 4.5 µL of cDNA and 0.5 µL of primer per reaction. All analysis were done relative to *Gapdh* or *Hprt*. Primer sequences can be found in Supplementary-Table S1.

ELISA

Cecal samples were collected from mice and stored at −80 °C until needed. Samples were prepared for ELISA as previously reported[67]. Briefly, frozen cecal samples were thawed and homogenized in PBS containing 0.1% Tween 20 at a concentration of 100 mg/mL. Homogenates were then centrifuged for 10 min and 12,000 rpm to remove solid debris. Clear supernatant was collected and utilized for experimentation with Mouse Lipocalin-2/NGAL DuoSet ELISA kit (R&D Systems) or Mouse Albumin ELISA Kit (RayBiotech) as per manufacture's protocol.

Tissue samples were collected, immediately flash frozen in liquid nitrogen, and stored at −80 °C until needed. Samples were homogenized for ELISA in tissue protein extraction buffer containing 100 mM Tris (pH 7.4), 150 mM NaCl, 1 mM EDTA, 1% triton, 0.5% sodium deoxycholate, 1 x protease inhibitor, phosphate inhibitor, and 1 mM Phenylmethylsulfonyl fluoride (PMSF). Homogenates were then centrifuged at 17,000 x *g* for 20 min at 4 °C and clear supernatant was collected. Protein concentration was determined via Pierce™ BCA Protein Assay Kits (23225). Equivalent amounts of protein was the

https://doi.org/10.1038/s41467-026-70479-z

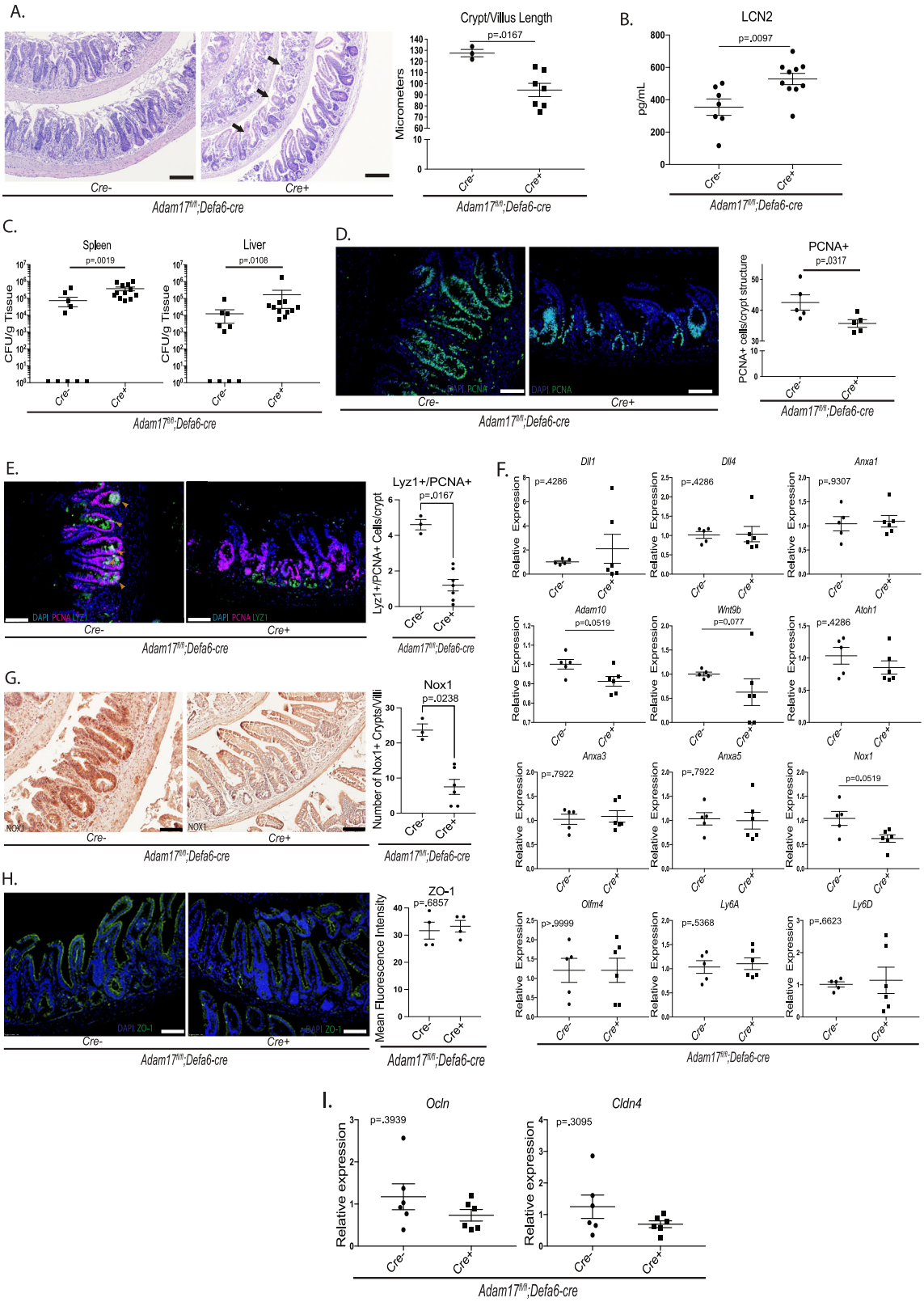

utilized for experimentation with the Mouse Epiregulin ELISA Kit (RayBiotech) as per the manufacture's protocol.

Histopathology

Terminal ileum tissue samples were prepared into Swiss roles, fixed in 10% formalin overnight and embedded in paraffin blocks. Paraffin embedded blocks were cut into 5 micron sections and adhered onto charged slides. Samples were then deparaffinized via Xylene and rehydrated via a descending ethanol gradient (100%, 95%, 70%, pure dH2O). For hematoxylin and eosin (H&E) staining, tissues were submerged in hematoxylin (VWR) for 5 minutes. Slides were then submerged in 3% acetic acid for 1 min. Slides were then washed under running tap water for approximated 15 min. Tissues were then submerged in eosin (VWR) for approximately 1 minute. Slides were then

Fig. 7 | ADAM17 signaling in Paneth cells contribute to intestinal regeneration after radiation induced injury. A Representative images of hematoxylin and eosin staining of terminal ilea from *Adam17$^{fl/fl}$;Defa6-cre* + /− mice 5 days post irradiation (scale bar = 100 µm) (left). Quantification of crypt lengths (right). Mice were 14.9 and 16 weeks old. *N* = 10. **B** Amounts of lipocalin in the cecal content of 5 day post irradiated *Adam17$^{fl/fl}$;Defa6-cre* + /− mice measured via ELISA. Mice were 6.9, 7 and 16 weeks old. *N* = 17. **C** Splenic and hepatic bacterial dissemination from *Adam17$^{fl/fl}$;Defa6-cre* + /− mice 5 days post irradiation. Mice were 6.9, 7 and 16 weeks old. *N* = 21. **D** Representative immunofluorescent images depicting PCNA (green) and DAPI (blue) from the ileum of *Adam17$^{fl/fl}$;Defa6-cre* + /− mice 5 days after irradiation (scale bar = 50 µm) (left) and quantification (right). Mice were 8.4, 14.9 and 16 weeks old. *N* = 10. **E** Representative immunofluorescent images depicting Lyz1 (green), PCNA (red) and DAPI (blue) from the ileum of *Adam17$^{fl/fl}$;Defa6-cre* + /− mice 5 days after irradiation (scale bar = 50 µm) (left) and quantification (right). Mice were 14.9 and 16 weeks old. *N* = 10. **F** RT-qPCR analysis depicting *Dll1, Dll4, Anxa1, Anxa3, Anxa5, Nox1, Adam10, Wnt9b, Atoh1, Olfm4, Ly6a*, and *Ly6d* expression in the terminal ileum from *Adam17$^{fl/fl}$;Defa6-cre* + /− mice 5 days post irradiation. Mice were 6.9 and 7 weeks old. *N* = 11. **G** Representative immunohistochemistry images depicting NOX1 from the ileum of *Adam17$^{fl/fl}$;Defa6-cre* + /− mice 5 days after irradiation (scale bar = 50 µm) (left) and quantification (right). Mice were 14.9, and 16 weeks old. *N* = 9. **H** Representative immunofluorescent images depicting ZO-1 (green) and DAPI (blue) from the ileum *Adam17$^{fl/fl}$;Defa6-cre* + /− mice 5 days after irradiation (scale bar = 50 µm) (left). Quantification via mean fluorescence intensity (right). *N* = 8. **I** RT-qPCR results from *Adam17$^{fl/fl}$;Defa6-cre* + /− mice 5 days post irradiation depicting *Ocln* and *Cldn4*. Mice were 6.9 and 7 weeks old. *N* = 12. *N* = number of biologically independent mice. All experiments are representative of 3 experiments. Data are presented as ± SEM on relevant graphs. (Mann-Whitney test, Two-tailed).

submerged in 95% and 100% ethanol successively for 2 min. Slides were then mounted using toluene and imaged using an Olympus CKX41 microscope. Crypt lengths were measured via the program ImageJ.

Immunofluorescence

Terminal ileum tissue samples were prepared into Swiss roles, fixed in 10% formalin overnight and embedded in paraffin blocks. Paraffin embedded blocks were cut into 5 micron sections and adhered onto charged slides. Samples were then deparaffinized via Xylene and rehydrated via a descending ethanol gradient (100%, 95%, 70%, pure dH2O). Antigen retrieval was performed by heating slides in a steamer for 40 minutes. Tissues were then submerged under 1x PBS containing 0.1% Triton X-100 (Sigma-Aldrich) for 10 min and then washed three times with 1X PBS containing 0.01% Tween 20 (VWR) to be permeabilized. Tissued were then blocked by 1x PBS containing 5% fetal bovine serum at 34 °C for 1 h. Following blocking, tissues were submerged in 1 x PBS containing 5% fetal bovine serum with primary anti-bodies against LYZ1-FITC (1:200) (Dako: F037201), PCNA (1:200) (Santa Cruz: sc-56), GFP (1:100) (Cell Signaling: 295SS), MUC2 (1:200) (Abcam: ab272692), DCLK1 (1:200) (Cell Signaling: 62257S), ADAM17 (1:200) (Invitrogen: MA5-32572), RFP (1:200) (Rockland: 200-101-379), UEA1-Dylight 649 (1:200) (Vector: DL-1068), IL-17RA (1:200) (Abcam: ab180904), ChGA (1:200) (Santa Cruz: sc-393941), I-FABP (1:200) (Santa Cruz: sc-374482) and ZO-1 (1:200) (Invitrogen: 61-7300) at 4 °C overnight. The next day, slides were washed three times with 1x PBS, the sections were incubated for 30 min at room temperature with Alexa Fluor® 488 AffiniPure™ Goat Anti-Rabbit IgG (H + L) (1:200) (Jackson ImmunoResearch: 111-545-144), Alexa Fluor® 647 AffiniPure™ F(ab')$_2$ Fragment Goat Anti-Rabbit IgG (H + L)(1:200) (Jackson ImmunoResearch: 111-606-144), Alexa Fluor® 488 AffiniPure™ F(ab')$_2$ Fragment Goat Anti-Mouse IgG (H + L) (1:200) (Jackson ImmunoResearch: 115-546-003), or Alexa Fluor® 647 AffiniPure™ F(ab')$_2$ Fragment Donkey Anti-Goat IgG (H + L) (1:200) (Jackson ImmunoResearch: 705-606-147). Slides were then mounted with DAPI hard mount (Southern Biotech), and images were acquired using an Olympus CKX41 microscope.

Organoids were lifted using ice-cold 1X PBS. Organoids were fixed in 4% paraformaldehyde for 15 min. Organoids were then washed with 1X PBS and permeabilized with .01% triton in 1X PBS for 10 min. After permeabilization, organoids were washed with 1X PBS and then blocked in 1X PBS containing 5% BSA for 1 hour at 34 °C. After blocking, organoids were incubated overnight at 4 °C in 1X PBS containing 5% BSA with primary antibodies against GFP (1:100) (Rockland: 600-901-215), Muc2 (1:200) (Santa Cruz: sc-515032), or ChGA (1:200) (Santa Cruz: sc-393941). The next day, organoids were washed with 1X PBS and then incubated for 30 min at 37 °C in 1X PBS containing 5% BSA with secondary antibodies Alexa Fluor® 488 AffiniPure™ F(ab')$_2$ Fragment Donkey Anti-Chicken IgG (H + L) (1:100) (Jackson ImmunoResearch: 703-544-155) and Alexa Fluor® 647 AffiniPure™ F(ab')$_2$ Fragment Donkey Anti-Mouse IgG (H + L) (1:200) (Jackson ImmunoResearch: 715-605-150). Organoids were then washed with 1X PBS and mounted on slides with DAPI hard mount (Southern Biotech), and images were acquired using an Olympus CKX41 microscope.

Live fluorescent murine organoids endogenously expressed fluorescence and thus were directly imaged in culture using an EVOS M5000 imaging system.

Immunohistochemistry

Paraffin embedded blocks were cut into 5 micron sections and adhered onto charged slides. Samples were then deparaffinized via Xylene and rehydrated via a descending ethanol gradient (100%, 95%, 70%, pure dH2O). Antigen retrieval was performed by heating slides in a steamer for 40 minutes. Tissues were then incubated in hydrogen peroxide block (abcam: 58661) for 10 minutes at room temperature. Sections were then washed in MilliQ water 2 times for 5 minutes followed by 1 wash in 1X TBS-T for 5 minutes. Sections were then blocked for 1 h at room temperature in 5% BSA in 1X TBS-T. Sections were then washed and avidin biotin block was performed as per the manufacturers protocol (Vector: SP-2001). Sections were then incubated overnight at 4 °C in 1X TBS-T containing primary antibody against Nox1 (1:250) (Proteintech: 17772-1-AP). The next day, section were washed 3 times in 1X TBS-T. Sections were then incubated at room temperature for 30 min in horse anti-rabbit IgG (H + L), biotinylated, R.T.U. (Vector: BP-1100). Sections were then washed in 1X TBS-T 3 times. Sections were then incubated in VECTASTAIN Elite ABC reagent, Peroxidase, R.T.U. (PK-7100) for 30 minutes at room temperature. Sections were then washed and then incubated in DAB (Dako: K3467) as per manufacturers protocol. Sections were then rinsed with MilliQ water and washed 3 times in 1X TBS-T for 5 min. Sections were then washed in MilliQ water and then counterstained with hematoxylin for 5 min Slides were then washed under running tap water for approximated 15 minutes. Slides were then submerged in 95% and 100% ethanol successively for 2 min. Slides were then mounted using toluene and imaged using an Olympus CKX41 microscope. Crypt lengths were measured via the program ImageJ.

TEM

Transmission electron microscopy was performed as previously described[68]. Briefly, terminal ileum samples were fixed in Karnovsky's Fixative (Electron Microscopy Sciences) overnight. The next day, tissues were incubated in 1% osmium tetroxide in 0.1 M PBS pH 7.4 and then dehydrated via a descending ethanol gradient. Dehydrated tissues were then embedded in EMbed 812 resin. 80 nm sections were then cut and placed on formvar-coated slot copper grids and counter stained using uranyl acetate and lead citrate. A FEI Tecnai12 BioTwinG2 transmission electron microscope was used to visualize tissues, and an AMT XR-60 CCD Digital Camera system was used to acquire images.

Acid-urea polyacrylamide gel electrophoresis (AU-PAGE)

Intestinal crypts were isolated as described. Crypts were then resuspended in 30% acetic acid and sonicated. After sonication, lysates were incubated overnight at 4 °C with agitation. Samples were then diluted threefold and centrifuged with a speed of 100,000 x *g* at 4 °C for 2 hours to remove insoluble material. Supernatant was collected, and protein concentration was determined via Pierce™ BCA Protein Assay Kits (23225). Equivalent amounts of protein were then lyophilized. The lyophilized protein was then dissolved in 30 µL of AU-PAGE loading buffer (3 M urea in 5% (v/v) glacial acetic acid in H_2O and methyl green). Equivalent amounts of protein was then loaded into AU-PAGE gels and run in 5% acetic acid running buffer with reverse polarity. Gels were run at 150 V until proteins reached the bottom. Proteins were then visualized via Coomassie blue staining and densitometry was performed via ImageJ.

Lymphocyte isolation

Lymphocytes were isolated as previously described[69]. Briefly, the small intestines were opened, Peyer's patched and luminal contents were removed, and the tissues were cut into ~ 2 cm pieces. To isolate lamina propria (LP) lymphocytes, the tissues were treated with EDTA (Invitrogen) solution at 37 °C with shaking at 220 rpm for 30 min to remove intestinal epithelial cells. The tissues were then digested with Type I collagenase (Gibco) at 37 °C with shaking at 300 rpm for 40 min and mashed through 70 µm cell strainers. LP lymphocytes were subsequently isolated using a 44%/67% Percoll gradient.

Flow cytometry

Intestinal crypts were isolated as described. Crypts were incubated in DMEM/F12 supplemented with 10% fetal bovine serum for 20 minutes at 4 °C. Crypts were then disassociated in TrypLE (Invitrogen) with 10 µM Rock inhibitor (Y-27632) and 2.5 µg/ml DNAse 1 (Sigma-Aldrich) for 10 min at 37 °C. Single cells were then washed twice in PBS. The following fluorophore-conjugated antibodies were purchased from Invitrogen: anti-CD24 (M1/69), anti-CD45 (30-F11), and anti-Epcam (G8.8). Live/Dead aqua fluorescent reactive dye was purchased from Invitrogen. Cells were then stained with antibodies for 30 minutes at 4 °C and filtered to remove clumps. Results were acquired with a BD-LSR-Fortessa, or cells were sorted using a FACS ARIA IIIU or a CytoFLEX SRT cell sorter.

Lymphocytes were isolated as described. The following fluorophore-conjugated antibodies were purchased from Biolegend, BD Biosciences or eBioscience: anti-CD45 (30-F11), anti-CD3ε (145-2C11), anti-CD19 (6D5), anti-CD11b (Mac-1), anti-Ly6C (HK1.4), anti-Ly6G (1A8), anti-CD64 (S18017D), anti-CD11c (N418), anti-MHC II (M5/114.15.2), anti-NK1.1 (PK136), anti-CD49b (DX5), anti-CD8α (53-6.7), anti-CD103 (2E7), anti-CD127 (A7R34), anti-RORγt (AFKJS-9), anti-Thy1.2 (30-H12), anti-CD4 (RM4-5) and anti-TCRβ (H57-597). Live/Dead dye was purchased from Invitrogen. Cells were incubated with antibodies for 30 min at 4 °C in the dark. For transcriptional factor staining, Foxp3/Transcription Factor Staining Buffer set (Invitrogen) was used according to the manufacturer's instructions. Samples were acquired on Aurora (Cytek), and data were analyzed using the FlowJo v.10 software (FlowJo, LLC).

Total RNA Sequencing (RNA-seq)

RNA sequencing and data analysis was performed as previously described[68]. Before constructing the Illumina TruSeq Total RNA library, total RNA was quantified using the Qubit RNA BR assay kit (Thermo Fisher Scientific: Guide MAN0001987 MP10210, Kit #Q10210). RNA quality was assessed on an Agilent 4150 Tapestation (G2992AA) with the Agilent RNA ScreenTape Analysis (Agilent: Publication Part Number: G2991-90021, Kit #5067-5576). A total of 2.5 µg of RNA was treated with 1 MBu Baseline-Zero DNase (Epicenter Cat. No DB0711K) according to the Baseline–Zero DNase protocol (www.epicentre.com, Lit # 263). The RNA was then purified and concentrated using 1.8 × volume Agencourt RNAClean XP Beads (Beckman Colter A63987) following the standard protocol (Protocol 001298v001). RNA concentration was re-measured with the Qubit BR RNA assay kit to prepare for input into the TruSeq Stranded Total RNA library protocol.

Illumina-compatible cDNA libraries with RiboZero Gold depletion were constructed according to the TruSeq Stranded Total RNA Reference Guide (Illumina Document #1000000040499v00, TruSeq Stranded Total RNA Gold Illumina Kit #20020598). Final cDNA library concentrations were determined using the Qubit dsDNA BR assay kit (Thermo Fisher Scientific: Guide MAN0002325 MP 32850, Kit #Q32850). The quality of the libraries was evaluated by running each on an Agilent 4150 Tapestation using the DNA 1000 Screentape kit (Agilent: Publication Part Number: G2991-90031, Kit #5067-5583). The electropherogram of each library was analyzed using Agilent 4150 Tapestation Analysis Software (Version 3.1) with a range of 200–600 bp to determine the average library size. Average size and concentration were used to calculate the molarity of each library. Libraries were pooled and denatured according to the Illumina Denature and Dilute Libraries Guide for the NextSeq System (Illumina Part #15048776). The denatured libraries were loaded onto an Illumina NextSeq 550 v2.5 Mid 150 output reagent cartridge (Illumina #20024904) at a final concentration of 1.5 pM in HT1 buffer, with 1% PhiX control library v3 (Illumina #FC-110-3001) added. Paired-end 75 bp single-index sequencing was performed, generating approximately 7.5 million paired-end reads per sample.

Sequencing analysis was carried out using RNA-seq for Eukaryotes Analysis v3 by the Banana Slug Genomics Center at the University of California, Santa Cruz. Raw paired-end sequencing reads from the Illumina sequencer were assessed for potential issues and contaminants using FastQC. Adapter sequences and primers were removed from the reads using Trimmomatic, followed by trimming of polyA tails, polyN sequences, and any reads with quality scores below 28 using PRINSEQ. Any reads shorter than 20 bp after trimming were discarded. A second round of quality control with FastQC was performed to compare read quality before and after trimming. The trimmed reads were mapped to the reference genome (GRCm38/mm10) using TopHat2, with NCBI RefSeq annotated genes as the transcriptome index. Read alignment coverage and summary statistics were computed using SAMtools, BEDtools, and UCSC Genome Browser utilities. For abundance estimation and differential expression analysis, the Cufflinks 2.2.0 workflow and read-counting methods using DESeq and edgeR were employed. Specifically, the sequencing reads aligned to RefSeq annotated genes were quantified using Cuffquant, and gene expression levels across the samples were normalized using Cuffnorm with FPKM values computed for sample correlation assessment. Differential expression analysis was performed using Cuffdiff on the results from Cuffquant. Additionally, HTSeq was used to compute raw read counts for the annotated RefSeq genes. Raw read counts were normalized across all samples and used for differential expression analysis with edgeR.

16S Microbial sequencing

Mouse cecal samples were collected and stored at − 80 °C. Cecal samples were shipped on ice. Fecal DNA was extracted via Qiagen DNeasy PowerLyser PowerSoil Kit (Qiagen). The bead beating step was performed following the manufacturer's instructions (PowerLyzer 24 Homogenizer, Omni International). The 16S microbial sequencing was performed as previously described[70].

AD-Adam17 and Ad-Y5 infection

HEK293 cells were infected with 100 MOI of with either Ad-Adam17 or Ad-Y5 overnight and were harvested for RT-PCR to confirm upregulation. Ad-Adam17 and Ad-Y5 were generated as previously described[71].

Mice were injected intraperitoneally with either Ad-Adam17 or Ad-Y5 at a concentration of 1×10^9 pfu/mouse. Mice were then irradiated 6 days post injection and processed as described above.

ADAM17 Activity assay

ADAM17 Fluorogenic Kit (BPS Bioscience) was utilized for ADAM17 activity assays as per manufacture's protocol. Briefly, ADAM17 protein was incubated at room temperature for 30 minutes with or without 4 mM H_2O_2. ADAM17 fluorogenic substrate was then added and results were collected every 10 minutes for 250 min utilizing an HTS 7000 Bio Assay Reader.

Statistical analysis

Bacterial dissemination, RT-qPCR, ELISA and all counting experiments were analyzed via non-parametric Mann-Whitney test, two tailed or Welch's *t* test using GraphPad/Prizim. Paired samples were analyzed via Wilcox test using GraphPad/Prizim. Grouped experiments were performed via two way ANOVA. Outliers were determined by using GraphPad Prism (ROUT analysis, Q = 1%). More specific statistical analysis details can be found in the figure legend of each figure. Cell counts were performed from at least 30 crypts per mouse.

Microbiome analysis was performed in R (version 4.3.1). Data was formatted utilizing phyloseq (version 1.44.0). Specifically, to normalize data, we filtered taxa with a relative abundance of < 1e-4, Total Sum Scaled (TSS) abundances to 1e6, and performed a general log transformation.

We calculated the beta diversity metric, Weighted UniFrac, and identified significance, using ADONIS, with the vegan package (version 2.6.6.1). To calculate LEfSe, we utilized the microbiomeMarker (version 1.6.0) package. All plots were created with ggplot2 (version 3.5.1).

Reporting summary

Further information on research design is available in the Nature Portfolio Reporting Summary linked to this article.

Data availability

The 16S rRNA microbial sequencing data are deposited in the Sequence Read Archive. The RNA-sequencing data from small intestinal tissues of *Il17ra*$^{fl/fl}$*; Defa6-cre* mice are deposited in the Sequence Read Archive. Both data are available under the ascension number PRJNA1368900 [https://www.ncbi.nlm.nih.gov/sra?LinkName=bioproject_sra_all&from_uid=1368900]. Previously published sequencing data can be found in GEO Relevant data underlying all non-sequencing-related findings are available in the Source Data file. Any additional information is available upon request to the corresponding author (Pawan Kumar, pawan.kumar@stonybrook.edu). Source data are provided in this paper.

References

1. Salzman, N. H. et al. Enteric defensins are essential regulators of intestinal microbial ecology. *Nat. Immunol.* **11**, 76–83 (2010).
2. Sato, T. et al. Paneth cells constitute the niche for Lgr5 stem cells in intestinal crypts. *Nature* **469**, 415–418 (2011).
3. Vaishnava, S., Behrendt, C. L., Ismail, A. S., Eckmann, L. & Hooper, L. V. Paneth cells directly sense gut commensals and maintain homeostasis at the intestinal host-microbial interface. *Proc. Natl. Acad. Sci. USA* **105**, 20858–20863 (2008).
4. Sailaja, B. S., He, X. C. & Li, L. The regulatory niche of intestinal stem cells. *J. Physiol.* **594**, 4827–4836 (2016).
5. Liu, T.-C. et al. Paneth cell defects in Crohn's disease patients promote dysbiosis. *JCI Insight.* **1**, https://doi.org/10.1172/jci.insight.86907 (2016).
6. Lueschow, S. R. & McElroy, S. J. The Paneth cell: the curator and defender of the immature small intestine. *Front. Immunol.* **11**, 1–12 (2020).
7. Clevers, H. C. & Bevins, C. L. Paneth cells: maestros of the small intestinal crypts. *Annu. Rev. Physiol.* **75**, 289–311 (2013).
8. Bevins, C. L. & Salzman, N. H. Paneth cells, antimicrobial peptides and maintenance of intestinal homeostasis. *Nat. Rev. Microbiol.* **9**, 356–368 (2011).
9. Schmitt, M. et al. Paneth cells respond to inflammation and contribute to tissue regeneration by acquiring stem-like features through SCF/c-kit signaling. *Cell Rep.* **24**, 2312–2328.e7 (2018).
10. Yu, S. et al. Paneth cell multipotency induced by notch activation following injury. *Cell Stem Cell* **23**, 46–59 (2018).
11. Ayyaz, A. et al. Single-cell transcriptomes of the regenerating intestine reveal a revival stem cell. *Nature* **569**, 121–125 (2019).
12. Jones, J. C. et al. Cellular plasticity of Defa4 cre -expressing Paneth cells in response to notch activation and intestinal injury. *Cmgh* **7**, 533–554 (2019).
13. Lin, X. et al. IL-17RA-signaling in Lgr5+ intestinal stem cells induces expression of transcription factor ATOH1 to promote secretory cell lineage commitment. *Immunity* **55**, 237–253.e8 (2022).
14. Haber, A. L. et al. A single-cell survey of the small intestinal epithelium. *Nature* **551**, 333–339 (2017).
15. Chang, S. H. & Dong, C. Signaling of Interleukin-17 family cytokines in immunity and inflammation. *Cell Signal* **23**, 1069–1075 (2011).
16. Dong, C. Regulation and pro-inflammatory function of interleukin-17 family cytokines. *Immunol. Rev.* **226**, 80–86 (2008).
17. Yao, Z. et al. Molecular characterization of the human interleukin (IL)-17 receptor. *Cytokine* **9**, 794–800 (1997).
18. Cua, D. J. & Tato, C. M. Innate IL-17-producing cells: The sentinels of the immune system. *Nat. Rev. Immunol.* **10**, 479–489 (2010).
19. Martin, D. A. et al. The emerging role of IL-17 in the pathogenesis of psoriasis: Preclinical and clinical findings. *J. Invest. Dermatol.* **133**, 17–26 (2013).
20. Fujino, S. et al. Increased expression of interleukin 17 in inflammatory bowel disease. *Gut* **52**, 65–70 (2003).
21. Targan, S. R. et al. A randomized, double-blind, placebo-controlled phase 2 study of brodalumab in patients With moderate-to-severe Crohn's disease. *Am. J. Gastroenterol.* **111**, 1599–1607 (2016).
22. Song, X. et al. Growth factor FGF2 cooperates with interleukin-17 to repair intestinal epithelial damage. *Immunity* **43**, 488–501 (2015).
23. Lee, J. S. et al. Interleukin-23-Independent IL-17 production regulates intestinal epithelial permeability. *Immunity* **43**, 727–738 (2015).
24. Maxwell, J. R. et al. Differential roles for interleukin-23 and interleukin-17 in intestinal immunoregulation. *Immunity* **43**, 739–750 (2015).
25. Kumar, P. et al. Intestinal interleukin-17 receptor signaling mediates reciprocal control of the gut microbiota and autoimmune inflammation. *Immunity* **44**, 659–671 (2016).
26. Tetteh, P. W. et al. Replacement of lost Lgr5-positive stem cells through plasticity of their enterocyte-lineage daughters. *Cell Stem Cell* **18**, 203–213 (2016).
27. Yan, K. S. et al. Intestinal enteroendocrine lineage cells possess homeostatic and injury-inducible stem cell activity. *Cell Stem Cell* **21**, 78–90 (2017).
28. Yu, J. Intestinal stem cell injury and protection during cancer therapy. *Transl. Cancer Res.* **2**, 384–396 (2013).
29. Moschen, A. R., Adolph, T. E., Gerner, R. R., Wieser, V. & Tilg, H. Lipocalin-2: A master mediator of intestinal and metabolic inflammation. *Trends Endocrinol. Metab.* **28**, 388–397 (2017).
30. Lu, F., Inoue, K., Kato, J., Minamishima, S. & Morisaki, H. Functions and regulation of lipocalin-2 in gut-origin sepsis: A narrative review. *Crit. Care.* **23**, 1–8 (2019).
31. Metcalfe, C., Kljavin, N. M., Ybarra, R. & De Sauvage, F. J. Lgr5+ stem cells are indispensable for radiation-induced intestinal regeneration. *Cell Stem Cell* **14**, 149–159 (2014).

32. Polistena, A. et al. Local radiotherapy of exposed murine small bowel: Apoptosis and inflammation. *BMC Surg.* **8**, 1–7 (2008).
33. François, A., Milliat, F., Guipaud, O. & Benderitter, M. Inflammation and immunity in radiation damage to the gut mucosa. *Biomed. Res. Int*. https://doi.org/10.1155/2013/123241 (2013).
34. Díaz-Díaz, L. M., Rodríguez-Villafañe, A. & García-Arrarás, J. E. The role of the microbiota in regeneration-associated processes. *Front. Cell Dev. Biol*. **9**, https://doi.org/10.3389/fcell.2021.768783 (2022).
35. Alam, A. et al. The microenvironment of injured murine gut elicits a local pro-restitutive microbiota. *Nat. Microbiol*. **1**, https://doi.org/10.1038/nmicrobiol.2015.21 (2016).
36. Montenegro-Miranda, P. S. et al. A novel organoid model of damage and repair identifies HNF4α as a critical regulator of intestinal epithelial regeneration. *Cmgh* **10**, 209–223 (2020).
37. Carulli, A. J. et al. Notch receptor regulation of intestinal stem cell homeostasis and crypt regeneration. *Dev. Biol*. **402**, 98–108 (2015).
38. Blaydon, D. C. et al. Inflammatory skin and bowel disease linked to ADAM17 deletion. *N. Engl. J. Med*. **365**, 1502–1508 (2011).
39. Viragova, S., Li, D. & Klein, O. D. Activation of fetal-like molecular programs during regeneration in the intestine and beyond. *Cell Stem Cell* **31**, 949–960 (2024).
40. Babbin, B. A. et al. Annexin A1 regulates intestinal mucosal injury, inflammation, and repair. *J. Immunol*. **181**, 5035–5044 (2008).
41. Yui, S. et al. YAP/TAZ-Dependent reprogramming of colonic epithelium links ECM remodeling to tissue regeneration. *Cell Stem Cell* **22**, 35–49 (2018).
42. Dang, M. et al. Regulated ADAM17-dependent EGF family ligand release by substrate-selecting signaling pathways. *Proc. Natl. Acad. Sci. USA* **110**, 9776–9781 (2013).
43. Baumgart, A. et al. ADAM17 regulates epidermal growth factor receptor expression through the activation of Notch1 in non-small cell lung cancer. *Cancer Res.* **70**, 5368–5378 (2010).
44. Wang, X. et al. ADAM17 variant causes hair loss via ubiquitin ligase TRIM47–mediated degradation. *JCI Insight*. **9**, https://doi.org/10.1172/jci.insight.177588 (2024).
45. Li, R. et al. High glucose up-regulates ADAM17 through HIF-1a in mesangial cells. *J. Biol. Chem.* **290**, 21603–21614 (2015).
46. Lian, G. et al. Macrophage metabolic reprogramming aggravates aortic dissection through the HIF1α-ADAM17 pathway☆. *EBioMedicine* **49**, 291–304 (2019).
47. Wang, H. P. et al. Nox1 promotes colon cancer cell metastasis via activation of the ADAM17 pathway. *Eur. Rev. Med. Pharmacol. Sci.* **20**, 4474–4481 (2016).
48. van der Post, S., Birchenough, G. M. H. & Held, J. M. NOX1-dependent redox signaling potentiates colonic stem cell proliferation to adapt to the intestinal microbiota by linking EGFR and TLR activation. *Cell Rep.* **35**, 108949 (2021).
49. Brill, A. et al. Oxidative stress activates ADAM17/TACE and induces its target receptor shedding in platelets in a p38-dependent fashion. *Cardiovasc. Res.* **84**, 137–144 (2009).
50. Wang, Y., Herrera, A. H., Li, Y., Belani, K. K. & Walcheck, B. Regulation of mature ADAM17 by redox agents for L-selectin shedding. *J. Immunol*. **182**, 2449–2457 (2009).
51. Terrill, J. R., Radley-Crabb, H. G., Grounds, M. D. & Arthur, P. G. N-Acetylcysteine treatment of dystrophic mdx mice results in protein thiol modifications and inhibition of exercise induced myofibre necrosis. *Neuromuscul. Disord.* **22**, 427–434 (2012).
52. Lee, S. I. & Kang, K. S. N-acetylcysteine modulates lipopolysaccharide-induced intestinal dysfunction. *Sci. Rep.* **9**, 1–10 (2019).
53. Malagola, E. et al. Isthmus progenitor cells contribute to homeostatic cellular turnover and support regeneration following intestinal injury. *Cell* **187**, 3056–3071 (2024).
54. Stalin, J. et al. Targeting of the NOX1 / ADAM17 enzymatic complex regulates soluble MCAM-dependent pro-tumorigenic activity in colorectal cancer. *Biomedicines*. **11**, https://doi.org/10.3390/biomedicines11123185 (2023).
55. Sisto, M., Lisi, S., Massimo, D. & Lofrumento, D. D. No TitleThe metalloproteinase ADAM17 and the epidermal growth factor receptor (EGFR) signaling drive the inflammatory epithelial response in Sjögren's syndrome. *Clin. Exp. Med.* **15**, 215–225 (2014).
56. Stanic, B., Katsuyama, M. & Miller, F. J. An oxidized extracellular oxidation-reduction state increases Nox1 expression and proliferation in vascular smooth muscle cells via epidermal growth factor receptor activation. *Arterioscler. Thromb. Vasc. Biol.* **30**, 2234–2241 (2010).
57. Xu, H. et al. Characterization and analysis of the temporal and spatial dynamic of several enteritis modeling methodologies. *Front. Immunol.* **12**, 1–17 (2021).
58. Lu, Q. et al. Radiation-induced intestinal injury: injury mechanism and potential treatment strategies. *Toxics* **11**, 1–23 (2023).
59. Liao, Z., Hu, C. & Gao, Y. Mechanisms modulating the activities of intestinal stem cells upon radiation or chemical agent exposure. *J. Radiat. Res.* **63**, 149–157 (2022).
60. Brabec, T. et al. IL-17-driven induction of Paneth cell antimicrobial functions protects the host from microbiota dysbiosis and inflammation in the ileum. *Mucosal Immunol*. **16**, 373–385 (2023).
61. Barker, N. et al. Identification of stem cells in small intestine and colon by marker gene Lgr5. *Nature* **449**, 1003–1007 (2007).
62. Yan, K. S. et al. The intestinal stem cell markers Bmi1 and Lgr5 identify two functionally distinct populations. *Proc. Natl. Acad. Sci. USA* **109**, 466–471 (2012).
63. Capdevila, C. et al. Time-resolved fate mapping identifies the intestinal upper crypt zone as an origin of Lgr5+ crypt base columnar cells. *Cell* **187**, 3039–3055 (2024).
64. Schmidt, S. et al. ADAM17 is required for EGF-R-induced intestinal tumors via IL-6 trans-signaling. *J. Exp. Med.* **215**, 1205–1225 (2018).
65. Saad, M. I. & Jenkins, B. J. The protease ADAM17 at the crossroads of disease: revisiting its significance in inflammation, cancer, and beyond. *FEBS J.* **291**, 10–24 (2024).
66. Shadad, A. K., Sullivan, F. J., Martin, J. D. & Egan, L. J. Gastrointestinal radiation injury: symptoms, risk factors and mechanisms. *World J. Gastroenterol*. **19**, 185–198 (2013).
67. Chassaing, B. et al. Fecal lipocalin 2, a sensitive and broadly dynamic non-invasive biomarker for intestinal inflammation. *PLoS ONE* **7**, 3–10 (2012).
68. Gaudino, S. J. et al. IL-22 receptor signaling in Paneth cells is critical for their maturation, microbiota colonization, Th17-related immune responses, and anti-Salmonella immunity. *Mucosal. Immunol.* **14**, 389–401 (2021).
69. Qiu, Z. & Sheridan, B. S. Isolating lymphocytes from the mouse small intestinal immune system. *J. Vis. Exp.* **2018**, 1–9 (2018).
70. Shahi, S. K., Zarei, K., Guseva, N. V. & Mangalam, A. K. Microbiota analysis using two-step pcr and next-generation 16s rrna gene sequencing. *J. Vis. Exp.* **2019**, https://doi.org/10.3791/59980 (2019).
71. Luo, J. et al. A protocol for rapid generation of recombinant adenoviruses using the AdEasy system. *Nat. Protoc.* **2**, 1236–1247 (2007).

Acknowledgements

We would like to acknowledge the Stony Brook University Histology core for paraffin imbedding of tissues in our study. We would also like to acknowledge the University of Iowa Microbiome Core for 16S microbiome sequencing and analysis. This work was supported by Crohn's and Colitis Foundation (476637 & 1168040), NIH R01 DK121798-01, NIH R21 AI146696, NIH AI149257 to PK, NIHDK088199 to RB, R01DK109559 (STM), R01DK115806 (STM), T32-GM133364 (KAB), 1F31DK136305 (KAB), Katherine E. Bullard Charitable Trust for Gastrointestinal Stem Cell and

Regenerative Research (S.T.M.), NRSA T32 training grant (T32AI007539) to S.J.G. Research reported in this publication was supported by the National Institute of General Medical Sciences of the National Institutes of Health under Award Number K12GM102778 (CGK). This work was also supported by T32GM127253 through the Stony Brook Scholars in Biomedical Sciences program (CGK).

Author contributions

P.K conceptualized the idea. C.G.K. and P.K. designed the experiments. C.G.K and P.K wrote the manuscript. C.G.K., S.J.G., and A.S. performed key experiments and data analyses. C.G.K. performed all irradiation and dissemination experiments. C.G.K., S.J.G., O.E., S.B., and T.B. performed organoid cultures, stimulation, and analysis. C.G.K., E.O., and A.B.B. performed all immunofluorescence staining. C.G.K. and A.S performed H&E staining and data analysis. C.G.K. performed all RT-qPCR experiments. C.G.K., A.S., S.J.G., Y.Y, and B.S.S. performed and analyzed all flow cytometry data. K.A.B. and S.T.M performed single-cell RNAseq analyses. R.B. and R.M. provided critical mice. P.H. provided AD- and Ad5. P.D. provided critical organoid samples and other materials. H.I.T. and K.S. performed genotyping on mice. P.K., P.D., A.B.B., S.T.M., H.K.K., B.S.S., S.B., and P.D. discussed data and commented on the manuscript, including critical revision of the manuscript.

Competing interests

The authors declare no competing interests.

Additional information

Supplementary information The online version contains supplementary material available at https://doi.org/10.1038/s41467-026-70479-z.

Correspondence and requests for materials should be addressed to Pawan Kumar.

Peer review information *Nature Communications* thanks the anonymous reviewers for their contribution to the peer review of this work. A peer review file is available.

[1]Department of Microbiology and Immunology, Stony Brook University, Stony Brook, NY, USA. [2]Department of Cell Biology & Physiology, University of North Carolina at Chapel Hill, Chapel Hill, NC, USA. [3]Department of Pediatrics, Renaissance School of Medicine, Stony Brook University, Stony Brook, NY, USA. [4]Cold Spring Harbor Laboratory, Cold Spring Harbor, NY, USA. [5]Department of Gastroenterology, Brigham and Women Hospital, Boston, MA, USA. [6]Department of Surgery, Stony Brook University, Stony Brook, NY, USA. [7]Department of Microbiology and Immunology, Virginia Commonwealth University, Richmond, VA, USA. [8]Department of Medicine, Renaissance School of Medicine, Stony Brook University, Stony Brook, NY, USA. [9]Joint Department of Biomedical Engineering, University of North Carolina at Chapel Hill and North Carolina State University, Raleigh, NC, USA. [10]Department of Medicine, University of North Carolina at Chapel Hill, Chapel Hill, NC, USA. [11]Center for Gastrointestinal Biology and Disease, University of North Carolina at Chapel Hill, Chapel Hill, NC, USA. [12]Department of Pediatrics, University of Colorado, Denver, CO, USA. ✉e-mail: pawan.kumar@stonybrook.edu